Dibaryon resonances and short-range *NN* interaction*

V.I. Kukulin# V.N. Pomerantsev† O.A. Rubtsova‡ M.N. Platonova§ I.T. Obukhovsky♮

Skobeltsyn Institute of Nuclear Physics, Lomonosov Moscow State University, Leninskie Gory 1/2, 119991 Moscow, Russia

Abstract: The dibaryon concept for nuclear force is presented, assuming that the attraction between nucleons at medium distances is mainly due to the *s*-channel exchange of an intermediate six-quark (dibaryon) state. To construct the respective *NN* interaction model, a microscopic six-quark description of the *NN* system is used, in which symmetry aspects play a special role. It is shown that the *NN* interaction in all important partial waves can be described by the superposition of long-range *t*-channel one-pion exchange and *s*-channel exchange by an intermediate dibaryon. The model developed in this study provides a good description of both elastic phase shifts and inelasticities of *NN* scattering in all *S*, *P*, *D*, and *F* partial waves at energies from zero to 600–800 MeV and even higher. The parameters of the intermediate six-quark states, corresponding to the best fit of *NN* scattering data, are found to be consistent with the parameters of the known dibaryon resonances in those *NN* partial configurations, where their existence has been experimentally confirmed. Predictions for new dibaryon states are given as well.

Keywords: nucleon-nucleon interaction, dibaryon resonances, short-range nuclear force

DOI: 10.1088/1674-1137/ac82e3

I. INTRODUCTION

It is now generally accepted that fundamental quantum chromodynamics (QCD) forms the basis of nuclear physics and determines its basic phenomena and laws, such as the nature of nuclear forces, specific structure of nuclei, observed features of nuclear reactions, etc. However, the direct connection between QCD and nuclear physics is hidden behind the complicated dynamics of quarks and gluons in the non-perturbative region, where there is a highly non-trivial relation between the completely different degrees of freedom of QCD and nuclear physics. While QCD operates with quarks and gluons, in traditional nuclear physics we deal with nucleons, mesons, and nucleon isobars.

Although there are many QCD-motivated models, which can reproduce the basic properties of baryons and mesons, so far there are no quantitative approaches to connect the observable properties of *NN* and 3*N* interactions, like *NN* scattering phase shifts and inelasticities, binding energies of two- and few-nucleon systems, etc., with the underlying properties of QCD. There are a few quark models that describe *NN* elastic scattering (see, e.g., the reviews [1, 2]); however, there are only a few (if any) quark-model approaches for describing both elastic and inelastic *NN* collisions above the pion-production threshold. Moreover, the quark models that have been developed thus far do not provide a quantitative description of the nuclear phenomena.

Thus, the constituent quark model (CQM), which uses the QCD-motivated quark-quark interaction, quite successfully describes the phase shifts of *NN* elastic scattering below the pion production threshold (and also the deuteron properties), based on calculations made within the resonating group method (RGM). In this case, the mixing of quark configurations and the connection of the *NN* channel with other cluster channels ($N\Delta$, $\Delta\Delta$, NN^*) play a crucial role [2]. Without taking these effects into account, the description of *S* and *D* waves would not be satisfactory. In addition, an adequate description of the triplet *P* and *F* waves has not yet been obtained. No RGM calculations have been performed above the pion production threshold. Moreover, it is clear that with increasing energy, the role of virtual clusters will increase, and they will make a non-trivial contribution to the production of real baryons. It is unlikely that the calculations of such in-

Received 11 May 2022; Accepted 21 July 2022

* The work has been partially supported by RFBR, grants Nos. 19-02-00011 and 19-02-00014. M.N.P. also appreciates support from the Foundation for the Advancement of Theoretical Physics and Mathematics "BASIS"

Deceased

† E-mail: pomeran@nucl-th.sinp.msu.ru

‡ E-mail: rubtsova-olga@yandex.ru

§ E-mail: platonova@nucl-th.sinp.msu.ru

♮ E-mail: obukh@nucl-th.sinp.msu.ru

elastic processes could be realized starting from the pair qq interactions. In contrast, the model proposed in this paper is effective for calculating both elastic and inelastic phase shifts in an energy range from zero to approximately 1 GeV. Additionally, instead of using a set of $3q-3q$ virtual cluster channels, it uses only one additional channel with a $6q$ dibaryon, which has the quantum numbers, mass, and width of the actually observed (or predicted) resonances.

The six-quark (or dibaryon) resonances can serve as an effective tool to relate the world of QCD with that of two- and few-nucleon dynamics. The dibaryon resonances, which are essentially multi-quark objects, reflect the very complicated dynamics of quarks and gluons in their structure. Meanwhile, when considered as dinucleon systems, they reflect the basic properties of the short-range NN interaction. Hence, the dibaryon (more generally, multi-baryon) resonances can be considered as appropriate effective degrees of freedom to describe the nuclear-physics phenomena, which involve the short-range NN interaction [3]. It should be emphasized here that dibaryon resonances can provide considerable information for understanding the short-range forces of NN, $N\Delta$, $\Delta\Delta$, etc., not only due to their structure, but essentially because they are specific, relatively long-lived, states in which six-quark dynamics should be manifested. It should be also noted that in the majority of the experimental and theoretical studies conducted previously, the non-trivial hexaquark states have been treated as something exotic, like penta- or tetraquarks, which are not related directly to the basic mechanism of the NN interaction.

The existence and main properties of some dibaryon resonances have now been reliably confirmed in numerous experimental and theoretical studies (see the recent reviews [4–6]). It should be noted that the history of dibaryon resonances has been very dramatic, from the initial enthusiasm through years of skepticism or even complete rejection until the final discovery in a series of precise high-statistics experiments made by several international collaborations (CELSIUS/WASA, WASA-at-COSY, ANKE-COSY, and others).

The dibaryon concept for the nuclear force based on an idea of the s-channel exchange dominance, originally proposed in Ref. [7], turned out to be very fruitful resulting in the construction of the dibaryon model (initially called the "dressed bag model") for the NN interaction [8, 9]. To keep the connection with the conventional meson-exchange ideas, the long-range part of the interaction was treated via the one-pion-exchange potential (OPEP). At the same time, the traditional t-channel multi-meson exchanges at short NN distances were replaced by the s-channel mechanism corresponding to the exchange of the dibaryon resonance (the $6q$ bag dressed with meson fields) between the interacting nucleons. Such a replacement looks quite natural in the two-nucleon overlap region and implements the duality principle for NN scattering (see, e.g., Ref. [10]). Moreover, this helps in overcoming many difficulties and inconsistencies in the coupling constants, cut-off parameters, etc., which persist in the meson-exchange approaches (for a detailed discussion on this issue, see, e.g., Ref. [11]). The initial version of the dibaryon model provided a very good description for NN elastic phase shifts in the lowest partial waves at energies up to 600 MeV (lab.), as well as the deuteron properties [8, 9]. A review of successes and consequences of the dressed bag model can be found in Ref. [12]. However, the parameters of the resonance poles obtained in this initial model have never been compared with the parameters of dibaryon resonances deduced from experimental data by the partial-wave analysis (PWA) or phenomenological models.

Recently, we extended the dibaryon model [8, 9] to higher partial waves and took into account inelastic processes (see Refs. [13–16]). This new version of the model makes it possible to describe both elastic and inelastic NN scattering in a wide energy range, far above the pion production threshold, and to reproduce (or predict) the empirical parameters of dibaryon resonances.

The main goal of the present study is to demonstrate that the NN interaction, in all important partial waves, can be described properly by a superposition of the long-range t-channel one-pion exchange and the s-channel exchange by an intermediate dibaryon state. We argue that the s-channel mechanism proposed here not only looks more natural but can also effectively replace the conventional t-channel multi-meson exchange at short distances (in the two-nucleon overlap region). We present the modified version of the dibaryon model and perform a comprehensive analysis of NN scattering in the framework of this model, including a number of partial-wave configurations not considered in previous works. We should emphasize that our purpose is not to prove the existence of dibaryon resonances, but to use them for construction of some alternative picture of the NN interaction and then compare their parameters with those deduced from experimental data. The success of this picture does not mean that one should reject the huge progress achieved within the conventional approaches. The short-range NN interaction can be actually described in different ways, but the QCD-motivated approach presented here has a wider range of applicability since it is free of some limitations inherent to the existing quark-model or meson-exchange treatments.

The structure of the paper is as follows. In Sec. II, we outline the modern experimental status of dibaryon resonances and their possible theoretical interpretation. In Sec. III, we describe the basic assumptions of the dibaryon concept and the tools needed for constructing the model for the NN interaction. Here, we introduce the two-chan-

nel formalism for the NN system with an additional internal channel corresponding to the quark degrees of freedom and present the basic results of the $6q$ microscopic consideration for the NN system. In particular, we demonstrate that all possible $6q$ states can be divided into states with a $6q$ bag structure with no leading hadronic configuration and two-cluster states with the dominating configurations of NN, $N\Delta$, $\Delta\Delta$, etc. In Sec. IV, we derive the effective Hamiltonian of the dibaryon model using a simple one-pole approximation for the internal channel resolvent. In Sec. V, the latest version of the model, which accounts for inelastic processes, is described, and the results of phase shifts calculations, inelasticities, and resonance parameters for the particular NN partial waves are presented. In Sec. VI, we summarize our results and provide the conclusions. In Appendices A and B, for the readers' convenience, we briefly reproduce the quark-model calculations of the transition form factors and vertex functions for the effective Hamiltonian, following Ref. [9].

II. MODERN STATUS AND STRUCTURE OF DIBARYONS

In this section, we give a brief review of the modern status of dibaryon resonances, from experimental and theoretical points of view. This is needed to substantiate the dibaryon concept for the NN interaction described in the next sections. For a more comprehensive review, see Refs. [4–6].

A. Modern status of dibaryon resonances

1. *Resonances predicted by Dyson and Xuong*

The first theoretical prediction for the existence of hexaquark (or dibaryon) resonances was done by Dyson and Xuong [17] in 1964, i.e., very soon after a pioneer work of Gell-Mann about quarks. By using the $SU(6)$ symmetry, the authors [17] predicted three pairs of low-lying non-strange dibaryon states near NN, $N\Delta$ and $\Delta\Delta$ thresholds. Denoted by $\mathcal{D}_{TJ}$, where T and J represent the isospin and total angular momentum, respectively, there were $\mathcal{D}_{01}$ (the deuteron) and $\mathcal{D}_{10}$ (the singlet deuteron), $\mathcal{D}_{12}$ and $\mathcal{D}_{21}$, and $\mathcal{D}_{03}$ and $\mathcal{D}_{30}$ states. Based on the simple $SU(6)$ mass formula and using the known masses of the first two trivial dibaryons, Dyson and Xuong predicted the masses of the other four states. Five out of the above six dibaryons have now been confirmed by experiments, which revealed surprisingly good agreement of the observed dibaryon masses with the above predictions.

In fact, the resonance peak located slightly below the $N\Delta$ threshold and having a width close to that of Δ, was observed well before the prediction of Dyson and Xuong in the experiments made by the group of Meshcheryakov *et al*. at the Dubna Synchrocyclotron [18, 19] on the reaction $\pi^+ d \to pp$. The follow-up PWA [20–27] confirmed the $\mathcal{D}_{12}$ dibaryon resonance in the reaction $\pi^+ d \to pp$ and revealed it also in pp and πd elastic scattering. The resonance pole corresponding to the average mass of about 2160 MeV and width of about 120 MeV was also found in the recent Faddeev calculations of the πNN system [28, 29]. Theoretically, it can be interpreted as an $N\Delta$ molecular-like state, though some admixture of hexaquark components is not excluded as well.

Some indication of the resonance $\mathcal{D}_{03}$ (denoted also by $d^*(2380)$) was found already in the early experiments [30, 31] on the reaction $np \to d\gamma$. However, just the recent series of high-statistics measurements, made first by the CELSIUS-WASA and then by the WASA-at-COSY Collaborations [32–37] on pn-induced double-pion production and np elastic scattering, left no doubt in the existence of the $T(J^P) = 0(3^+)$ dibaryon state with the mass 2380 MeV (i.e., 80 MeV below the $\Delta\Delta$ threshold) and rather narrow width of about 70 MeV. The $d^*(2380)$ resonance was also confirmed in the deuteron photodisintegration measurements by the A2 Collaboration at MAMI [38, 39]. The resonance pole corresponding to the $d^*(2380)$ state was found in the PWA [35–37] and confirmed by the Faddeev calculations of the $\pi N\Delta$ system [28–29]. The subsequent quark-model calculations (e.g., [40–42]) explained the observed mass and width of the dibaryon as being due to the dominance of the six-quark hidden-color (CC) components in this state. For now, it appears to be the only known dibaryon state having predominantly hexaquark (i.e., not molecular-like) structure [5]. One should note also a recent attempt to explain the observed properties of interacting $N\Delta$ and $\Delta\Delta$ systems without the need for any six-quark states, based on the coupled-channel calculation accounting for the Fermi motion in these systems [43]. Such a consideration, however, gives too narrow widths of the observed $\mathcal{D}_{12}$ and $\mathcal{D}_{03}$ states and does not agree with some of the experimental mass distributions [5].

Two resonances with the mirrored quantum numbers, i.e., $\mathcal{D}_{21}$ and $\mathcal{D}_{30}$, have been actively searched for in the recent WASA-at-COSY experiments on the $pp \to pp\pi^+\pi^-$ and $pp \to pp\pi^+\pi^+\pi^-\pi^-$ reactions, respectively. The evidence for the first resonance with the mass and width very close to those of the $\mathcal{D}_{12}$ state has been actually found [44, 45]. This resonance has also been predicted in the Faddeev calculations [28, 29]. For the $\mathcal{D}_{30}$ state, only upper limits have been found so far [46]. Hence, this dibaryon state should be investigated further.

2. *Other isovector resonances*

In the late 1970s, the whole series of isovector dibaryon resonances in the channels with $L = J$ ($^1D_2$, $^3F_3$, $^1G_4$, $^3H_5$, etc.) were discovered in double-polarized $\vec{p}+\vec{p}$ scat-

tering (i.e., the spin-polarized beam was scattered on the spin-polarized target) [47–52]. The subsequent analysis [53] showed that these diproton resonances can be arranged to lie on a straight-line trajectory in the $L(L+1)-M_D$ plane, where L is the relative orbital angular momentum in the pp system. This straight-line trajectory was interpreted [53] as evidence of the rotational nature of these diproton resonances, very similar to the nuclear rotational bands. Soon after that, in 1980, the Nijmegen group (Mulders *et al.*) suggested the q^4-q^2 string-like model [54] for the six-quark states, which was generalized later by the ITEP group (Kondratyuk *et al.*) [55] with incorporation of the relativistic treatment and spin-orbit splitting in the $6q$ system. In terms of the Nijmegen–ITEP q^4-q^2 model, the above series of isovector dibaryons corresponds to the rotation of the two-cluster system with the color string connecting the q^4 and q^2 quark clusters on its ends.

The direct extrapolation of the trajectory for $L=0$ and $L=1$ gives the ${}^1S_0$ dibaryon shifted upwards by 145 MeV. This shift might be explained by the intermediate σ-meson production in the spin-singlet ${}^1S_0$ channel, which lowers the mass of the dibaryon (see Sec. II.B). The $L=1$ dibaryon should have the quantum numbers ${}^3P_1$ and the mass ~ 2060 MeV. Thus, this dibaryon could be identified by its mass with the d' resonance predicted in Ref. [55]. The corresponding resonance peak was observed in the exclusive measurements of the $pp\to pp\pi^+\pi^-$ reaction [56] but has not been confirmed by the succeeding experiments [57]. In fact, no clear signal of a dibaryon state in the ${}^3P_1$ channel has been detected to date. However, such a state (with a mass of about 2180 MeV) was found in the PWA [26, 27]. The recent calculations [16] within the dibaryon model have also shown that the existence of the ${}^3P_1$ dibaryon resonance with the mass of about 2200 MeV does not contradict the SAID PWA data [58]. However, these data are not sensitive enough to deduce the mass and width of the resonance unambiguously, so, the question about the existence of the ${}^3P_1$ resonance is still open.

On the other hand, the dibaryon resonances in the ${}^3P_0$ and ${}^3P_2$ channels with the mass of about 2200 MeV have been clearly found in the recent experiment of the ANKE-COSY Collaboration [59]. The authors [59] studied the reaction $pp\to(pp)_S\pi^0$, where $(pp)_S$ is a diproton in the near-threshold ${}^1S_0$ state. This reaction is complimentary to the reaction $pp\to d\pi^+$, where the isovector dibaryons ${}^1D_2$, ${}^3F_3$ and ${}^3P_2$ play an important role [60, 61]. The ${}^1D_2p$ and ${}^3F_3d$ transitions, which dominate the reaction with the final deuteron, are excluded by selection rules in the case of the final diproton. So, the largest contribution here is given by the amplitudes ${}^3P_0s$ and ${}^3P_2d$, both of which exhibit the pronounced resonance behavior. While the ${}^3P_2$ resonance was known previously from the PWA [24–27], the ${}^3P_0$ one has been found in Ref. [59] for the first time.

3. *Dibaryon masses and nucleon resonance thresholds*

Hadron and nuclear physics tell us that bound or resonance states generally appear near the thresholds. It seems true for the known dibaryon resonances as well. As was pointed out in Ref. [62] (see also [63]), there is a clustering effect for the isovector ${}^1D_2$, ${}^3F_3$ ${}^1G_4$, etc., states, as their masses are close to each other and to the $N\Delta$ threshold. Moreover, these states lie very close to the $N\Delta$ thresholds in the respective partial waves, when the orbital angular momentum is taken into account [64]. The P-wave states ${}^3P_0$ and ${}^3P_2$ found in Ref. [59] lie also near the $N\Delta$ threshold. At the same time, the isoscalar $d^*(2380)$ state is located rather close to the $\Delta\Delta$ threshold, while the "trivial" S-wave states ${}^3S_1$ (deuteron) and ${}^1S_0$ (singlet deuteron) lie near the NN threshold. Recently, two more dibaryon states near the $NN^*(1440)$ threshold have been found both in the WASA-at-COSY experiments on single- and double-pion production [65] and theoretical calculations of NN elastic scattering in S waves [15][1)].

In addition, two new isoscalar dibaryons at 2.47 and 2.63 GeV have been found in the recent measurements of double-pion photoproduction on the deuteron at ELPH (Tohoku) [67, 68]. The positions of these states correspond to the second and third nucleon resonance regions, respectively. The special kinematic constraints of the experiments [67, 68] made it possible to separate the dibaryon contributions from those of the nucleon resonances. The same experiments have also confirmed the $\mathcal{D}_{03}$ and $\mathcal{D}_{12}$ resonances. Very recently, one more isoscalar resonance has been found by the same group in the $\gamma d\to d\eta$ reaction [69]. This resonance with a mass of about 2.43 GeV and a narrow width of only 34 MeV lies near the $NN^*(1535)$ and $d\eta$ thresholds. A similar dibaryon state has been announced also by the ANKE-COSY Collaboration in $pn\to dX$ around the $d\eta$ threshold [70].

Thus, dibaryon resonances have been discovered to date in almost all basic NN partial channels. Moreover, there are indications (or evidences) of some states uncoupled from the NN channel, which can be manifested in the $NN\pi$, $NN\pi\pi$, etc., systems. All known dibaryon states are located near the respective di-hadron thresholds. These findings are very inspiring for searching new near-threshold dibaryons and developing the classification of these states to shed light on their microscopic structure.

1) The recent analysis suggests the dibaryon state found in the isoscalar single-pion production might be related predominantly to the ${}^1P_1$ rather than ${}^3S_1$ state [66]. This situation might be similar to that with several dibaryon states sitting on top of each other near the $N\Delta$ threshold.

B. Two-cluster q^4-q^2 model for dibaryon states and σ-meson emission

Among many theoretical models for dibaryon states, the closest one to our consideration is the Nijmegen – ITEP q^4-q^2 model [54, 55]. We started our six-quark studies from the other edge, i.e., using the quark shell-model representation (see details in Refs. [8, 9]) to describe the bag-like multi-quark states. Nevertheless, we found that the two completely different pictures above, i.e., the two-cluster $4q-2q$ and $6q$ shell-model representations, can be rewritten in a unified form. In fact, the leading shell-model $6q$ configuration $|s^4p^2[42]L=0,\,2;\,ST\rangle$ (written in a single-particle representation) can be transformed into the two-cluster $4q-2q$ form using the standard Talmi –Moshinsky transformation for the harmonic oscillator functions (h.o.f.):

$$|s^4p^2[42]LST\rangle \Rightarrow |s^4[4]L_0S_0T_0, s^2[2]lst(2\hbar\omega)L=0,2ST\rangle, \tag{1}$$

where the tetraquark $|s^4[4]L_0S_0T_0\rangle$ and diquark $|s^2[2]lst\rangle$ have the $2\hbar\omega$ relative-motion wavefunction and mutual orbital momenta $L=0,2$ allowable for a two-quanta excitation of the h.o.f. The most low-lying six-quark configurations correspond to the tetraquark having $L_0=0$, $S_0T_0=01$ or 10 and the diquark being in a scalar ($lst=000$) or axial ($lst=011$) states [55]. Two quark clusters are assumed to be connected by a color string with a $2\hbar\omega$ excitation energy. It can be interpreted as a $2\hbar\omega$ -vibration or a D-wave rotation of the string. Thus, it turns out that the quark-cluster model suggested by the Nijmegen and ITEP groups and our shell-model picture can be transformed into each other and interpreted in a unified way.

In turn, the $2\hbar\omega$-excited string can emit a scalar σ-meson and thus, the excited two-cluster $4q-2q$ state can transit into an unexcited bag-like configuration $|s^6[6]+\sigma,L\rangle$ with conservation of the orbital momentum L (see Fig. 1). In the quark shell-model representation, it corresponds to the transition of two p-shell quarks from the p to s orbit with the simultaneous emission of two tightly correlated s-wave pions. For instance, in S waves we have:

$$|s^4p^2[42]_xLST\rangle \to |s^6[6]+\sigma(l_\sigma=0)\rangle. \tag{2}$$

Thus, we identify the specific mechanism of the σ-meson emission from the excited dibaryons with the σ emission from the excited color string. Such a type of string transition, accompanied by the two-pion emission,

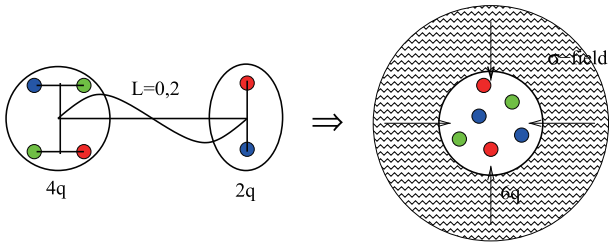

Fig. 1. (color online) Illustration for the transition of the $2\hbar\omega$-excited $6q$ state into the unexcited fully symmetric configuration $|s^6[6]+\sigma,L\rangle$ by emission of a scalar σ-meson from the excited color string.

appears to take place in hadronic processes, like the huge $2\pi^0$ production in the scalar mode in high-energy pp collisions [71], the 2π-decay of the Roper resonance, etc. Furthermore, we have shown recently that the emission of the σ meson from the intermediate dibaryon state can explain the long-term near-threshold anomaly (the so-called ABC effect) in two-pion production in pn, pd, etc., collisions at intermediate energies [72, 73].

It is also very interesting to identify this string de-excitation mechanism with the σ-meson emission via a monopole transition in the spectra of charmonium and bottomonium:

$$\Psi(2s)\to\Psi(1s)+2\pi^0,\ \Psi(3s)\to\Psi(2s)+2\pi^0,\ldots$$

$$\Upsilon(2s)\to\Upsilon(1s)+2\pi^0,\ \Upsilon(3s)\to\Upsilon(2s)+2\pi^0,\ldots$$

It is well known that these monopole transitions are associated with de-excitation of the string connecting q and $\bar{q}$ in quarkonia [74]. Thus, one can suggest, in particular, that two-pion production in high- or intermediate-energy NN collisions and the monopole transitions in the quarkonia spectra have the unified nature related to de-excitation of the color string.

Let us move one step further from the above six-quark picture to the properties of the NN interaction. The microscopic six-quark model predicts [75, 76] that the mixed-symmetry states $|s^4p^2[42]_xLST\rangle$ can be almost confluent to the fully symmetric states $|s^6[6]\rangle$, so that, they can mix to each other in the S-wave channels of NN scattering. In contrast, the mixed-symmetry $6q$ components can overpass to the fully symmetric ones by the σ emission. If the emitted σ meson has not very high energy and the transition occurs in the field of the multi-quark core, the final σ meson will attach to the fully symmetric $6q$ core and this will lead to a significant energy shift of the initial mixed-symmetry states[1)]. This energy shift results in a strong effective attraction in the respective NN channels.

1) The similar attachment of the σ meson to the fully symmetric $|s^3[3]\rangle$ core leads to the well-known mass shift of the Roper resonance which makes its Breit–Wigner mass (1440 MeV) ca. 500 MeV lower than the mass of the excited three-quark state $|sp^2[3]\rangle$.

These findings form a base for the QCD-motivated dibaryon model of the NN interaction, which we discuss below. In the model, the basic intermediate-range attraction between nucleons is a consequence of the formation of a six-quark bag dressed by the strong scalar σ field in NN collisions. It may seem that the physical σ meson (listed as $f_0(500)$ in the PDG tables [77]), which has a mass of about 500 MeV and a large width of the same order, can hardly play such a significant role in the NN interaction. However, it was shown in, e.g., Refs. [78–81], that the σ-meson mass and width can be strongly reduced, and thus it can become much more stable, due to the partial chiral symmetry restoration, which takes place in excited hadrons or dense baryon matter. We assume a similar mechanism to take place in the $6q$ states, which satisfy both these conditions due to their compact size (at least for some of the known dibaryons) and inner $2\hbar\omega$ excitation. Thus, we have shown in Refs. [72, 73] that the ABC effect in the $pn \to d\pi\pi$ reactions can be explained by the emission of the renormalized σ meson with the mass of about 300 MeV and width of about 100 MeV from the $d^*(2380)$ dibaryon state. In the initial version of the dibaryon model for the NN interaction [8, 9], we formally dealt with the stable light scalar mesons with the mass of about 300 – 350 MeV and zero width. We should note that the stable σ meson, as a pure phenomenological construction, has been commonly used in the traditional meson-exchange models for the NN interaction to account for the intermediate-range attraction. The intermediate dibaryon formation can at least partially substantiate the (relative) stability of the scalar mesons, which arise not in the empty space between two nucleons, but in the field of $6q$ states. The direct inclusion of the σ width in the model would strongly complicate the practical calculations and lead to arising of the complex potential, the imaginary part of which should be related to inelastic processes (mainly 2π production). In the present version of the model described below in Sec. V, we take into account the inelastic processes by introducing the dressed dibaryon width (which effectively includes the width of the σ meson within the dibaryon).

III. QUARK DEGREES OF FREEDOM IN THE TWO-NUCLEON SYSTEM

The dibaryon concept for the NN interaction, originally proposed in Ref. [7], and the dressed bag model developed on its basis in Refs. [8, 9], suggests the following picture of the interaction between nucleons. At relatively large distances ($r_{NN} > 1$ fm), nucleons interact by the traditional pion exchange. However, when nucleons approach each other at a distance of $r_{NN} \lesssim 1$ fm, a compound dibaryon state is formed, which can be described as a six-quark bag, dressed by meson fields, where the most important one is a field of light scalar σ mesons. As a result of multiple transitions of a two-nucleon system to the state of a dressed six-quark bag and vice versa, an effective interaction arises, which gives the main attraction between the nucleons at intermediate distances.

A. Formal scheme including internal and external spaces

To describe the mechanism of such an interaction, it is convenient to use a two-channel formalism, which assumes that a system of two nucleons can be in two different states (channels): an external NN channel and an internal dibaryon channel. The total wavefunction of such a system consists of two components belonging to two different Hilbert spaces. Thus, it can be written as a two-component column:

$$\Psi \in \mathcal{H} = \begin{pmatrix} \Psi^{\rm ex} \in \mathcal{H}^{\rm ex} \\ \Psi^{\rm in} \in \mathcal{H}^{\rm in} \end{pmatrix}.$$

The two Hilbert spaces, $\mathcal{H}^{\rm ex}$ and $\mathcal{H}^{\rm in}$, have quite different natures: $\Psi^{\rm ex}$ depends on the relative coordinate (or momentum) of two nucleons and their spins, whereas $\Psi^{\rm in}$ can depend on quark, gluon and meson variables of the internal state. The two independent Hamiltonians are defined in each of these spaces: $h^{\rm ex}$ acts in $\mathcal{H}^{\rm ex}$ and $h^{\rm in}$ acts in $\mathcal{H}^{\rm in}$.

The total Hamiltonian h acting in the total Hilbert space $\mathcal{H} = \mathcal{H}^{\rm ex} \oplus \mathcal{H}^{\rm in}$ can be written in a matrix form:

$$h = \begin{pmatrix} h^{\rm ex} & h^{\rm ex,in} \\ h^{\rm in,ex} & h^{\rm in} \end{pmatrix}, \tag{3}$$

where the transition operators $h^{\rm ex,in} = (h^{\rm in,ex})^\dagger$ determine the coupling between external and internal channels. Note that if operators $h^{\rm ex}$ and $h^{\rm in}$ are self-adjoint and $h^{\rm ex,in}$ is bounded, then the Hamiltonian h is the self-adjoint operator in $\mathcal{H}$.

The external Hamiltonian

$$h^{\rm ex} = t + v^{\rm ex}$$

includes the kinetic energy t of the NN relative motion and some peripheral part of the interaction $v^{\rm ex}$, i.e., the peripheral part of the meson-exchange potential and the Coulomb interaction in the case of two protons.

The total wavefunction Ψ satisfies the two-component Schrödinger equation

$$h\Psi = E\Psi. \tag{4}$$

By excluding the internal component, one obtains an effective Schrödinger equation for the external channel only:

$$h^{\rm eff}(E)\Psi^{\rm ex} = E\Psi^{\rm ex} \tag{5}$$

with an effective "pseudo-Hamiltonian"

$$h^{\rm eff}(E) = h^{\rm ex} + h^{\rm ex,in}\, g^{\rm in}(E)\, h^{\rm in,ex} = t + v^{\rm ex} + w(E), \tag{6}$$

which depends on energy[1)] E due to the resolvent of the internal Hamiltonian $g^{\rm in}(E) = (E - h^{\rm in})^{-1}$.

Having found the solution $\Psi^{\rm ex}$ of the effective equation (5), one can uniquely restore the excluded internal state:

$$\Psi^{\rm in} = g^{\rm in}(E) h^{\rm in,ex}\Psi^{\rm ex}. \tag{7}$$

To determine the components of the total Hamiltonian in the above formal scheme, it is necessary to use some microscopic theory, which, in principle, is able to describe both the external and internal channels and, most importantly, the transitions between them. A six-quark model was used for these purposes in Refs. [8, 9]. We briefly outline, below, the main assumptions and the resulting form of the dibaryon model following from the microscopic six-quark treatment of the *NN* system.

B. Six-quark structure of the two-nucleon system: symmetry aspects

Within the microscopic six-quark description, the RGM ansatz can be used for the *NN* -channel wavefunction:

$$\Psi^{\rm RGM}_{NN}(123456) = \mathcal{A}\{\psi_N(123)\psi_N(456)\chi_{NN}(\boldsymbol{r})\}, \tag{8}$$

where $\boldsymbol{r} = \frac{1}{3}(\boldsymbol{r}_1+\boldsymbol{r}_2+\boldsymbol{r}_3-\boldsymbol{r}_4-\boldsymbol{r}_5-\boldsymbol{r}_6)$ is the distance between the nucleon clusters, and $\psi_N(i,j,k)$ is the quark wavefunction of the nucleon:

$$\psi_N(123) = \varphi_N(\boldsymbol{\rho}_1,\boldsymbol{\xi}_1)\,|[1^3]_C S_{3q},([21]_{CS})T_{3q}:[1^3]_{CST}\rangle, \tag{9}$$

with $\boldsymbol{\rho}_1 = \boldsymbol{r}_1 - \boldsymbol{r}_2$, $\boldsymbol{\xi}_1 = \frac{1}{2}(\boldsymbol{r}_1+\boldsymbol{r}_2) - \boldsymbol{r}_3$, $S_{3q} = 1/2$, $T_{3q} = 1/2$, and $\mathcal{A}$ is the antisymmetrizer consisting of permutations of all six quarks.

Then the wavefunction in the external channel corresponds to the renormalized RGM relative-motion function [82]:

$$\Psi^{\rm ex}(\boldsymbol{r}) \to \mathcal{N}^{-1/2}\chi_{NN}(\boldsymbol{r}), \tag{10}$$

where $\mathcal{N}$ is the so-called overlap kernel:

$$\mathcal{N}(\boldsymbol{r}',\boldsymbol{r}) = \langle\psi_N\psi_N|\mathcal{A}\delta(\boldsymbol{r}'-\boldsymbol{r})|\psi_N\psi_N\rangle. \tag{11}$$

The external and transition Hamiltonians correspond to the following RGM expressions:

$$\begin{aligned} h^{\rm ex} \to h^{\rm ex}_{\rm RGM}(\boldsymbol{r}',\boldsymbol{r}) &= \langle\psi_N\psi_N|\mathcal{A}h^{\rm ex}_{6q}|\psi_N\psi_N\rangle, \\ h^{\rm ex,in} \to h^{\rm ex,in}_{\rm RGM}(\boldsymbol{r}';\boldsymbol{r},\{\boldsymbol{\rho}\boldsymbol{\xi}\}) &= \langle\psi_N\psi_N|\mathcal{A}h^{\rm ex,in}_{6q}, \end{aligned} \tag{12}$$

which include some microscopic $6q$ Hamiltonian. Here, for brevity, the set of inner coordinates of the six-quark system $\boldsymbol{r},\boldsymbol{\rho}_1,\boldsymbol{\xi}_1,\boldsymbol{\rho}_2,\boldsymbol{\xi}_2$ is denoted by $\boldsymbol{r},\{\boldsymbol{\rho}\boldsymbol{\xi}\}$.

Next, we consider the possible symmetry of the $6q$ wavefunctions in the framework of the translationally invariant shell model (TISM) including all $6q$ configurations with 0 $\hbar\omega$, 1 $\hbar\omega$, and 2 $\hbar\omega$ excitations. Let us consider the possible $6q$ spatial symmetries of the external *NN* channel, e.g., in the case of an *S* partial wave. If one assumes the symmetry of the nucleon wavefunction as $[f_X] = [3]_X$, then the allowed $6q$ symmetries in even partial waves should be $[6]_X$ and $[42]_X$. These two components should be associated with unexcited $|s^6[6]_X L = 0\rangle$ and excited $|s^4p^2[42]_X L = 0,2\rangle$ configurations, respectively. It was shown in Refs. [75, 76, 83] that the components of the first type should be identified with bag-like configurations, while the second-type components can be naturally identified with the proper *NN* configurations.

The quark wavefunction of the nucleon is a quark shell-model configuration $s^3[3]_X$ symmetric in the X (coordinate) space, and in the CST (color, spin, isospin) space. It is described by a specific set of Young schemes satisfying the Pauli principle:

$$\begin{aligned} |N\rangle &= |s^3[3]_X\rangle|N(CST)\rangle, \\ |N(CST)\rangle &= |[1^3]_{CST}\{[21]_{CS}([1^3]_C\circ[21]_S)\circ[21]_T\}\rangle. \end{aligned} \tag{13}$$

The $6q$ wavefunction of the *NN* system composed from the free-nucleon states (13) can be expanded (see the formalism in Refs. [84, 85]) in the quark shell-model configuration series, which includes both fully symmetric $s^6[6]_X$ and mixed-symmetry $s^5p[51]_X$, $s^4p^2[42]_X$, $s^3p^3[3^2]_X$ states. Here the s^6 and s^4p^2 configurations correspond to the even *NN* partial waves, while s^5p and s^3p^3 ones to the odd *NN* partial waves. It is important that the restrictions imposed by the Pauli principle in the mixed-symmetry states are not as stringent as in the case of the fully symmetric ones $[6]_X$, but still remain quite

1) From the mathematical point of view, an operator depending on the spectral parameter is not an operator at all, because its domain depends on this spectral parameter. Therefore, strictly speaking, such an object should not be called the Hamiltonian. However, physicists ignore this fact and use energy-dependent interactions very widely.

important for the "almost symmetric" Young scheme $[51]_X$.

The following basic sets of states satisfy the Pauli principle for the NN channels [75, 76, 86] (taking into account the requirement of color neutrality, $[1^3]_C \times [1^3]_C \to [2^3]_C$):

1. For even orbital momenta L (i.e., $ST = 10, 01$)

$$\Psi_0 = |s^6[6]_X L = 0; [1^6]_{CST} \times \{[2^3]_{CS}([2^3]_C \circ [42]_S) \circ [3^2]_T\}\rangle,\ ST = 10, \quad (14)$$

$$\Psi'_0 = |s^6[6]_X L = 0; [1^6]_{CST} \times \{[2^2 1^2]_{CS}([2^3]_C \circ [3^2]_S) \circ [42]_T\}\rangle,\ ST = 01, \quad (15)$$

and

$$\Psi_2^{(i)} = |s^4 p^2 [42]_X L = 0, 2; [2^2 1^2]_{CST} \times \{[f_2]_{CS}([2^3]_C \circ [42]_S) \circ [3^2]_T\}\rangle,\ ST = 10, \quad (16)$$

where $i = 1, 2, ..., 5$ is the number in the set of color-spin (CS) Young schemes:

$$[f_2]_{CS} (= [2^3]_C \circ [42]_S) = [42], [321], [2^3], [31^3], [21^4] \quad (17)$$

(here $[2^3]_C \circ [42]_S$ is the inner product of the color and spin Young schemes),

$$\Psi'^{(i)}_2 = |s^4 p^2 [42]_X L = 0, 2; [2^2 1^2]_{CST} \times \{[f'_2]_{CS}([2^3]_C \circ [3^2]_S) \circ [42]_T\}\rangle,\ ST = 01, \quad (18)$$

with $i = 1, ..., 4$ being the number in the set

$$[f'_2]_{CS} (= [2^3]_C \circ [3^2]_S) = [3^2], [41^2], [2^2 1^2], [1^6]. \quad (19)$$

2. For odd orbital momenta L (i.e., $ST = 11, 00$)

$$\Psi_1 = |s^5 p [51]_X L = 1; [21^4]_{CST} \times \{[\tilde{f}_1]_{CS}([2^3]_C \circ [42]_S) \circ [42]_T\}\rangle,\ ST = 11 \quad (20)$$

(here only the values $[\tilde{f}_1]_{CS} = [321], [2^3], [21^4]$ from the set (17) are allowed, while $[42]$ and $[31^3]$ are forbidden),

$$\Psi'_1 = |s^5 p [51]_X L = 1; [21^4]_{CST} \times \{[2^2 1^2]_{CS}([2^3]_C \circ [3^2]_S) \circ [3^2]_T\}\rangle,\ ST = 00, \quad (21)$$

and

$$\Psi_3^{(i)} = |s^3 p^3 [3^2]_X L = 1, 3; [2^3]_{CST} \times \{[f_3]_{CS}([2^3]_C \circ [42]_S) \circ [42]_T\}\rangle,\ ST = 11 \quad (22)$$

with $i = 1, 2, ..., 5$ being the number in the set (17),

$$\Psi'^{(i)}_3 = |s^3 p^3 [3^2]_X L = 1, 3; [2^3]_{CST} \times \{[f'_3]_{CS}([2^3]_C \circ [3^2]_S) \circ [3^2]_T\}\rangle,\ ST = 00 \quad (23)$$

with $i = 1, ..., 4$ being the number in the set (19).

One can see that the Pauli exclusion principle does not forbid the unexcited configurations $s^6[6]_X$ and $s^5 p[51]_X$ in the channels with positive and negative parity, respectively, but severely limits the set of allowable Young schemes in the CS subspace, reducing the allowed basis to only a single CS state $[2^3]_{CS}$ ($[2^2 1^2]_{CS}$) in even triplet (singlet) partial waves and strongly restricting the basis in odd partial waves. At the same time, the excited configurations $s^4 p^2 [42]_X$ and $s^3 p^3 [3^2]_X$ satisfy the Pauli principle for any value of the CS Young scheme from the Clebsch–Gordan series (17) and (19) for the inner product of color and spin Young schemes in the triplet ($S = 1$) and singlet ($S = 0$) channels. So, in a rough approximation, one can evaluate the short-range NN interaction by considering the configurations dominating in the overlap region of two nucleons.

In quark models using the QCD-induced interaction [87], viz., the confinement potential $\sim \lambda_i \lambda_j$ and the spin-dependent color-magnetic interaction $\sim \lambda_i \lambda_j \sigma_i \sigma_j$, the state with the most symmetric Young scheme $[42]_{CS}$ from the series (17) is marked out in energy. Note that the energy splitting between the states with the color-spin symmetry $[42]_{CS}$ and $[2^3]_{CS}$ is of the same order of magnitude as the $N - \Delta$ splitting (i.e., the splitting between the hadronic states with the color-spin symmetry $[21]_{CS}$ and $[1^3]_{CS}$). It is worth noting that, from the whole series (17), only the first term $[42]_{CS}$ corresponds to the state, in which the color-magnetic interaction term leads to the NN attraction in the overlap region [75, 76, 86]. In the singlet channel, the state with the most symmetric Young scheme $[3^2]_{CS}$ from the series (19) plays the same role. Consequently, the dominance of the configurations $s^4 p^2 [42]_X$ and $s^3 p^3 [3^2]_X$ over the more symmetric ones $s^6[6]_X$ and $s^5 p[51]_X$ in the overlap area can lead to the NN attraction instead of the strong short-range repulsion in the traditional approaches.

The numerical calculations [75, 76] of the NN elastic scattering within the RGM framework confirmed the above conclusions made from the symmetry considerations. In these calculations, the authors used the QCD-induced interaction and took into account the exchange of the Goldstone boson $\{\sigma, \boldsymbol{\pi}\}$ between quarks.

The six-quark RGM wavefunction of the NN system $\Psi_{NN} = \mathcal{A}\{\chi_{NN}(r; E) N(123) N(456)\}$, corresponding to the realistic description of the scattering phase shifts in the

$^3S_1$ wave in a wide energy range $0 < E \lesssim 1$ GeV, was projected onto the shell-mode $6q$ configurations $s^6[6]_X$ and $s^4p^2[42]_X$ by using the TISM methods. As a result, the following important representation was obtained for the microscopic wavefunction Ψ_{NN} [75, 76]:

$$\Psi_{NN}(^3S_1;E) = c_0(E)\Psi_0 + \Psi^Q_{NN}(^3S_1;E),$$
$$\Psi^Q_{NN}(^3S_1;E) = \sum_{i=1}^{5} c_2^{(i)}(E)\Psi_2^{(i)} + \mathcal{A}\{\chi^{ass}_{NN}(r;E)NN\}, \quad (24)$$

where the antisymmetrizer $\mathcal{A}$ was omitted before $6q$ configurations Ψ_n, since the basic states (14)–(23) are antisymmetric by definition:

$$\mathcal{A}\Psi_n = \Psi_n, \quad \mathcal{A}^2 = \mathcal{A}. \quad (25)$$

Note that the same expansion can also be written for the singlet S-wave NN channel:

$$\Psi'_{NN}(^1S_0;E) = c'_0(E)\Psi'_0 + \Psi'^Q_{NN}(^1S_0;E),$$
$$\Psi'^Q_{NN}(^1S_0;E) = \sum_{i=1}^{4} c_2'^{(i)}(E)\Psi_2'^{(i)} + \mathcal{A}\{\chi'^{ass}_{NN}(r;E)NN\}. \quad (26)$$

In both cases, the first term proportional to Ψ_0 (Ψ'_0) includes a coherent superposition of NN, $\Delta\Delta$ and CC states (see, e.g., the first column of Table A1 in Appendix A) with the large weight just for the CC component (states with the hidden color). Thus, this term likely corresponds to a $6q$ bag-like component.

The second term Ψ^Q_{NN} [Ψ'^Q_{NN}] includes a coherent superposition of five [four] components corresponding to the mixed-symmetry configurations $s^4p^2[42]_X$ [$s^3p^3[3^2]_X$] with all CS Young schemes from the series (17) [(19)]. This term has been demonstrated [75, 76] to correspond to a state vector where the cluster NN component (i.e., widely spaced and non-symmetrized product of the nucleonic wave functions) has the maximal weight, while the remaining components interfere destructively and, as a result, can only be considered as small corrections to the basic NN component. At the same time, the asymptotic part $\mathcal{A}\{\chi^{ass}_{NN}(r;E)N(123)N(456)\}$ of the cluster component Ψ^Q_{NN} is orthogonal to configurations Ψ_n and has only a minor effect on the short-range wavefunction [75, 76].

Thus, according to Refs. [75, 76], the quark-model wavefunction of NN scattering in the $^3S_1$ partial wave consists of two qualitatively different components: the shell-model state $s^6[6]_X$ symmetric in the coordinate space, like a $6q$ bag composed mainly from CC states and corresponding to the internal dibaryon channel, and the NN cluster-like state Ψ^Q_{NN} corresponding to $2\hbar\omega$ -excited relative motion of two nucleons at short distances (i.e., the external channel). By analogy, we may assume that the quark-model wavefunction of NN scattering in the $^1S_0$ partial wave also consists of two different components: the shell-model bag-like state $s^6[6]_X$ and the NN cluster-like state Ψ'^Q_{NN} . Therefore, the transition from the external NN component (mainly having the mixed symmetry) to the internal $6q$ bag components must be accompanied by a transition of two p-shell quarks to the s shell, with an emission of two tightly correlated pions.

The projection of the cluster component onto the NN channel in the overlap region $r \lesssim 2b$ (where b is the radius of nucleon "quark core"), at each fixed value of energy E, takes the form:

$$\sqrt{\frac{6!}{3!3!2!}}\langle NN|\sum_{i=1}^{5} c_2^{(i)}|\Psi_2^{(i)}\rangle = \mathcal{N}_0\left(1-\frac{r^2}{b^2}\right)\exp\left(-\frac{3r^2}{4b^2}\right) \quad (27)$$

(we should use the primed terms $c_2'^{(i)}\Psi_2'^{(i)}$ in the case of the $^1S_0$ wave). This relative-motion wavefunction has a radial node localized at the distance b. According to Refs. [75, 76], both components have approximately equal probabilities $\sum_{i=1}^{5}|c_2^{(i)}(E)|^2 \approx |c_0(E)|^2$ for any value of E in the interval $0 < E \lesssim 1$ GeV. Consequently, the node of the NN cluster part of the wavefunction (27) is almost independent on energy in this range. This means that only the normalization factor $\mathcal{N}_0$ in the r.h.s. of Eq. (27) is really dependent on energy up to ≈ 1 GeV.

C. The nodal structure of NN wavefunctions

The stationary node at the distances $r \approx b$ plays the same role in NN elastic scattering as the repulsive core in the traditional potential models for the NN interaction. In particular, the stationary node of the NN wavefunction completely explains the constant negative slope of the phase shifts in the $^3S_1$ ($^1S_0$) partial wave, up to energies $E \approx 1$ GeV.

As for the ^3D_J ($^1D_2$) partial waves, they correspond to the configuration $s^4p^2[42]_X(L=2)$ in the quark-model description. So, in the ^3D_J ($^1D_2$) channels, instead of Eqs. (24)–(26), one gets a similar expansion:

$$\Psi_{NN}(^3D_J;E) = \Psi^Q_{NN}(^3D_J;E)$$
$$= \sum_{i=1}^{5} d_{2J}^{(i)}(E)\Psi_{2DJ}^{(i)} + \mathcal{A}\{\chi^{ass}_{NNDJ}(r;E)Y_2(\hat{r})NN\}_J \quad (28)$$

for the triplet D waves and for the singlet D wave as well (with primed basis functions and primed coefficients).

Despite the fact that the expansions (24) and (28) seem very similar, they actually correspond to a different behavior of NN scattering phase shifts. This can be seen by projecting the cluster component $\Psi^Q_{NN}(^3D_J;E)$ onto the NN channel. Instead of the nodal function (27), one gets

a nodeless radial function

$$\sqrt{\frac{6!}{3!3!2!}}\langle NN|\sum_{i=1}^{5}d_2^{(i)}|\Psi_{2D}^{(i)}\rangle=\mathcal{N}_2\frac{r^2}{b^2}Y_2(\hat{r})\exp\left(-\frac{3r^2}{4b^2}\right). \quad (29)$$

Therefore, in contrast to the ${}^3S_1$ (${}^1S_0$) wave, the hard-core effects should not be manifested in the energy dependence of the ${}^3D_J$ (${}^1D_2$) phase shift. However, the spin-orbit interaction and tensor coupling in the triplet channel could modify the energy dependence of the ${}^3D_J$ phase shift as compared to our qualitative quark-model consideration accounting for the Pauli exclusion principle.

The situation with the triplet odd partial waves ${}^3P_J$ and ${}^3F_J$ looks a little bit more complicated than for even partial waves. In fact, the possible Young schemes for the orbital part of the $6q$ wavefunction in P waves are $s^5p[51]_X$ and $s^3p^3[33]_X$ with respective CS parts shown in Eqs. (20)–(23). Thus, we can assume that the wavefunction with the symmetry $s^5p[51]_X$, being the intermediate between the fully symmetric bag-like component $s^6[6]_X$ and the highly clusterized state $s^4p^2[42]_X$, should manifest some cluster-like properties, i.e., it can dissociate into the respective NN channel.

Meanwhile, in P waves, one should take into consideration the spin-orbit splitting even for the $6q$ wavefunction. Taking into account the spin-orbit splitting, one notes that $p_{\frac{3}{2}}$ quark orbit lies lower than $p_{\frac{1}{2}}$ orbit. Therefore, the $6q$ configuration $s^5p[51]_X$ includes just the $p_{\frac{3}{2}}$ single-quark orbit, i.e., it corresponds to the $s^5p_{\frac{3}{2}}[51]_X$ state, quite similarly to the nuclear physics case of the ^{5}Li and ^{5}He ground states (with the nuclear shell-model configuration $s^4p_{\frac{3}{2}}[41]_X$). In turn, the possible total angular momenta for the configuration $s^5p_{\frac{3}{2}}[51]_X$ are $J=2$ and $J=1$, but not $J=0$. In such a case, in the triplet NN channels ${}^3P_2-{}^3F_2$ and ${}^3P_1$, one has a superposition of two $6q$ components: $s^5p_{\frac{3}{2}}[51]_X+s^3p^3[33]_X$, while in the ${}^3P_0$ channel one has the nodal $s^3p^3[33]_X$ component only. Due to the presence of a radial node in the NN scattering wavefunction, this component corresponds to the strongly enhanced kinetic energy and thus induces some additional repulsion in the NN system.

Although, in general, the formalism for the odd partial waves ${}^3P_J-{}^3F_J$ and ${}^1P_1-{}^1F_3$ is more complicated, we use here the basis vectors from the set (20)–(23), in the same way as we used the states (14)–(18) for the even partial waves ${}^3S_1-{}^3D_J$ and ${}^1S_0-{}^1D_2$. First, we consider the basis of the state with the total orbital momentum $L=1$. The state with the Young scheme $[42]_{CS}$ apparently plays here the same role as in the ${}^3S_1-{}^3D_J$ channels. This can be seen from the comparison of the basis vectors (20), (22) and (14), (16). Therefore, it is also possible here to expand the quark wavefunction into an NN cluster part and a bag-like part with the more symmetric wavefunction in the coordinate space (its CST content is strongly limited by the Pauli principle):

$$\Psi_{NN}({}^3P_J;E)=\sum_{i=1}^{3}\tilde{p}_{1J}^{(i)}(E)\Psi_{1J}^{(i)}+\Psi_{NN}^{Q}({}^3P_J;E),$$

$$\Psi_{NN}^{Q}({}^3P_J;E)=\sum_{i=1}^{5}p_{3J}^{(i)}(E)\Psi_{3J}^{(i)}+\mathcal{A}\{\chi_{NNPJ}^{ass}(r;E)Y_1(\hat{r})NN\}_J. \quad (30)$$

Here, $\tilde{p}_{1J}^{(i)}(E)$ and $p_{3J}^{(i)}(E)$ are the expansion coefficients of the NN -scattering quark wavefunction (e.g., the solution of the RGM equation) with a given value of the total angular momentum $J=L+S$ (here $S=1$ and the obvious algebra of addition of momenta is omitted). In the overlap area $r\lesssim 2b$, the projection of the cluster component of the function (30) onto the NN channel, calculated by the TISM methods, must have a node at a distance $r=b$, regardless of the specific value of J, if there is no spin-orbit interaction.

$$\sqrt{\frac{6!}{3!3!2!}}\langle NN|\sum_{i=1}^{5}p_{3J}^{(i)}|\Psi_{3J}^{(i)}\rangle=\mathcal{N}_3\left(1-\frac{r^2}{b^2}\right)\frac{r}{b}Y_1(\hat{r})\exp\left(-\frac{3r^2}{4b^2}\right). \quad (31)$$

In reality, the spin-orbit interaction is present, and, as a result, the phase shifts in ${}^3P_J$ channels have significant splitting in J. Moreover, ${}^3P_0$ and ${}^3P_1$ phase shifts have a constant negative slope, which indicates the presence of a stable node in the cluster component of the quark wavefunction and the predominance of an attractive force at small distances. However, the behavior of the ${}^3P_2$ phase shift is different, which is possibly explained by the essential role of tensor mixing ${}^3P_2-{}^3F_2$.

Meanwhile, to rewrite the shell-model $6q$ wavefunctions $s^5p[51]_X$ and $s^3p^3[33]_X$ within the framework of the Nijmegen–ITEP $4q-2q$ model [54, 55] (see Sec. II.B), one gets a strong spin-orbit attraction in the component $|s^5p[51]_X,J=2\rangle$ and much weaker — in the component $|s^5p[51]_X,J=1\rangle$. Thus, the weight of the nodeless component $|s^5p[51]_X,J=2\rangle$ should be much higher than that of the $|s^5p[51]_X,J=1\rangle$ component, as compared with the contribution of the second (nodal) component $|s^3p^3[33]_X,J\rangle$.

As a result of this qualitative consideration, one can conclude that the NN radial wavefunction in the triplet ${}^3P_2$ channel should be predominantly nodeless with the main component $|s^5p[51]_X,J=2\rangle$. At the same time, for the ${}^3P_1$ channel, the situation is opposite, i.e., the $|s^3p^3[33]_X$, $J=1\rangle$ component should dominate. In the ${}^3P_0$ channel, the mixed-symmetry configuration $|s^3p^3[33]_X,J=0\rangle$ leads to the nodal radial wavefunctions. The empirical behaviour of the triplet P-wave phase shifts correspond ex-

actly to such a behaviour of quark wavefunctions, which follows from the microscopic consideration.

The situation in the triplet ${}^3F_J$ channels resembles the one in the ${}^3P_J$ channels: the p-shell states with the mixed-symmetry configuration $|s^3p^3[33]_X, J\rangle$, $J=2,3,4$, correspond to the nodal radial wavefunction, but in this case there should be an admixture of the f-shell states with an almost symmetric configuration $|s^5f[51]_X, J\rangle$ having the CS structure considerably restricted by the Pauli principle.

Hence, all the triplet odd partial waves ${}^3P_J$ and ${}^3F_J$ can be described by the dibaryon model for the NN interaction. The situation in the singlet odd channels ${}^1P_1$ and ${}^1F_3$ is simpler, since the spin-orbit splitting is absent here and there is only one bag-like state (21) in the P wave. Here, the expansion similar to Eq. (30) has the form:

$$\begin{aligned}&\Psi_{NN}({}^1P_1;E) = p_1'(E)\Psi_1' + \Psi_{NN}^{Q}({}^1P_1;E),\\ &\Psi_{NN}^{Q}({}^1P_1;E) = \sum_{i=1}^{4} p_3'^{(i)}(E)\Psi_3'^{(i)} + \mathcal{A}\{\chi_{NNP1}^{ass}(r;E)Y_1(\hat{r})NN\}_{J=1}.\end{aligned} \tag{32}$$

An analogous expansion is valid for $\Psi_{NN}({}^1F_3;E)$ with the substitution $p_1'(E)\to f_1'(E)$, $\Psi_1'\to\Psi_1''=|s^5f[51]_XL=3\rangle$, …, etc.

Thus, we have shown that just the mixed-symmetry states with the six-quark structure $|s^4p^2[42]_xLST\rangle$ dominate over the fully space-symmetric configuration $|s^6[6]\rangle$ due to a much higher statistical weight and specific features of the quark-quark interaction ($v_{qq}\sim\vec{\lambda}_i\vec{\lambda}_j\vec{\sigma}_i\vec{\sigma}_j$). When treating the S-wave NN interaction, this property leads to the presence of a stationary node in the NN radial wavefunctions in a broad energy range from zero to 1 GeV [75, 76].

The same property is also valid for the P-wave states of the $6q$ system, where the $|s^3p^3[33]_xLST\rangle$ configuration dominates over the $|s^5p[51]_xLST\rangle$ one. Hence, the NN scattering radial wavefunctions in such P waves must display a similar nodal behavior.

IV. EFFECTIVE HAMILTONIAN OF THE DIBARYON MODEL

Let us now turn to the formalism of the dibaryon model. After excluding the internal channel from the total Hamiltonian (3) acting in the two-component Hilbert space, one comes to an effective NN Hamiltonian (6):

$$h^{\rm eff}(E) = h^{\rm ex} + w(E), \tag{33}$$

where $w(E)=h^{\rm ex,in}\,g^{\rm in}(E)\,h^{\rm in,ex}$ is the effective energy-dependent interaction due to the coupling with the internal channel. We recall that the external Hamiltonian $h^{\rm ex}$ includes, in addition to the kinetic energy t, the peripheral meson-exchange interaction. Below, we show how the explicit form of the effective interaction $w(E)$ can be obtained from the microscopic quark consideration in the pole approximation.

A. The pole approximation for the resolvent of the internal Hamiltonian

A complete description of the internal channel, as a system of six interacting quarks surrounded by a meson field, is a complicated problem. However, to determine the effective potential $w(E)$ in the external NN channel, it is sufficient to take into account only one or few lowest states of the $6q$ bag, which leads to a simple pole approximation for the resolvent of the internal channel:

$$g^{\rm in}(E) = \sum_{\alpha}\int \frac{|\alpha,\boldsymbol{k}\rangle\langle\alpha,\boldsymbol{k}|{\rm d}^3k}{E-E_{\rm in}(\alpha,\boldsymbol{k})}, \tag{34}$$

where $|\alpha\rangle$ is the $6q$ part of the wavefunction for the dibaryon states. The plane waves $|\boldsymbol{k}\rangle$ describe the σ-meson states, whereas the total energy $E_{\rm in}(\alpha,\boldsymbol{k})$ of the dressed bag is:

$$E_\alpha(\boldsymbol{k}) = m_\alpha + \varepsilon_\sigma(k), \tag{35}$$

where

$$\varepsilon_\sigma(k) = k^2/2m_\alpha + \omega_\sigma(k) \simeq m_\sigma + k^2/2\bar{m}_\sigma, \tag{36}$$

$\omega_\sigma(k)=\sqrt{m_\sigma^2+k^2}$ is the relativistic energy of the σ meson, $\bar{m}_\sigma = m_\sigma m_\alpha/(m_\sigma+m_\alpha)$ is the reduced mass of the dressed bag and m_σ and m_α are the masses of the σ meson and the bare $6q$ bag, respectively.

Using the pole approximation (34) for $g^{\rm in}$, one can represent the effective interaction $w(E)$ as a sum of factorized terms:

$$w(E) = \sum_{\alpha}\int \frac{h^{\rm ex,in}|\alpha,\boldsymbol{k}\rangle\langle\alpha,\boldsymbol{k}|h^{\rm in,ex}\,{\rm d}^3k}{E-E_{\rm in}(\alpha,\boldsymbol{k})}. \tag{37}$$

Such an effective interaction $w(E)$, resulting from the coupling of the external NN channel to the dressed $6q$ bag, is illustrated in Fig. 2.

Since we have adopted the pole approximation (34) for the resolvent of the internal channel $g^{\rm in}$, the derivation of the effective interaction w in the external channel does not require the knowledge of the full internal Hamiltonian $h^{\rm in}$ of the dressed bag, nor the full transition operator $h^{\rm ex,in}$. As follows from Eq. (37), it is necessary to determine the result of the transition operator action

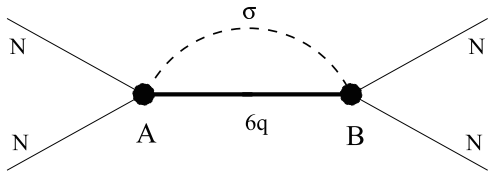

Fig. 2. Effective NN interaction induced by the formation of an intermediate $6q$ bag dressed by meson fields.

only on those states of the dressed bag $|\alpha,\boldsymbol{k}\rangle$, which we included in the resolvent $g^{\rm in}$.

If the RGM ansatz (8) is used to describe the external channel, then the action of the transition operator (12) on the state $|\alpha,\boldsymbol{k}\rangle$ can be formally written as:

$$h^{\rm ex,in}|\alpha,\boldsymbol{k}\rangle = \langle\{\psi_N\psi_N\}_{ST}|\hat{O}_\sigma(\boldsymbol{k},E)|\alpha,\boldsymbol{k}\rangle, \tag{38}$$

where $\hat{O}_\sigma(\boldsymbol{k},E)$ is an annihilation operator for the σ meson with the momentum $\boldsymbol{k}$ and the indices ST are the spin-isospin quantum numbers of the NN state [with the nucleon $3q$ wave function given by Eq. (9)].

The formal expression (38) already allows us to define the general structure of the transition vertex B in Fig. 2, without detailing the form of the operator $\hat{O}_\sigma(\boldsymbol{k},E)$. After the partial-wave decomposition of the r.h.s. in Eq. (38), one obtains (at a fixed orbital momentum of the σ meson L_σ):

$$h^{\rm ex,in}|\alpha\{S_\alpha,L_\sigma\}_{JM},k\rangle = \sum_L B^J_{L_\sigma LS}(k,E)|Z^{JM}_{LS}\rangle, \tag{39}$$

where the sum over L includes all the admissible values of NN orbital momenta compatible with the fixed value of J, L_σ and S_{6q} . The function $B^J_{L_\sigma LS}(k,E)$ is the vertex function in the transition $NN \leftrightarrow 6q+\sigma$ and $Z^{JM}_{LS} \in \mathcal{H}^{\rm ex}$ is the transition form factor in the NN channel.

It is essential that the form of the radial functions $Z^{JM}_{LS}(r)$ can be derived from the quark-model calculations in terms of the RGM ansatz. Moreover, the vertex functions $B^J_{L_\sigma LS}(k,E)$ can be also calculated within the same microscopic model [8, 9]. For the convenience of the reader, Appendices A and B provide a brief summary of the main assumptions and relationships used in the derivation of the functions $Z^{JM}_{LS}(r)$ and $B^J_{L_\sigma LS}(k,E)$ in Ref. [9].

After substituting Eq. (39) into Eq. (37), one obtains an effective potential $w(E)$ induced by coupling the external NN channel to the internal dibaryon channel in a form of a sum of simple separable terms for each partial wave:

$$w(E) = \sum_{S,J,L,L'} V^{SJ}_{LL'}(E), \tag{40}$$

with

$$V^{SJ}_{LL'}(E) = \sum_M |Z^{JM}_{LS}\rangle\, \lambda^J_{SLL'}(E)\, \langle Z^{JM}_{L'S}|, \tag{41}$$

where the energy-dependent coupling constants $\lambda^J_{SLL'}(E)$ are expressed in terms of the integral over the momentum k of the product of two transition vertices B and the convolution of the meson and quark propagators:

$$\lambda^J_{SLL'}(E) = \int_0^\infty k^2 {\rm d}k \frac{B^J_{L_\sigma LS}(k,E)\, B^J_{L_\sigma L'S}{}^*(k,E)}{E - E_\alpha(k)}. \tag{42}$$

Eqs. (40), (41) and (42) are the main result of the quark microscopic treatment for the NN interaction within the two-component formalism. One can see that incorporating the non-nucleon (dibaryon) components leads to an effective NN interaction $w(E)$, which has the form of a sum of separable terms with a specific energy dependence and which, in particular, can include the coupling between NN channels with different values of the orbital angular momentum L, i.e., tensor mixing.

B. A repulsive core effect in the external NN channel

As noted in Sec. III.B, the important feature of the suggested mechanism for the transition between the external and internal channels is the presence of two excited p-shell quarks in the incident NN channel, which go to the s shell with emission of two highly coherent pions (see Appendix B for details). Such a mechanism spans the transitions $s^4p^2 \to s^6$ and $s^3p^3 \to s^5p$ when the inner-channel states are described by the most symmetric configurations s^6 and s^5p in even and odd partial waves, respectively. In line with this assumption, we should primarily consider the states in the external NN channel, which correspond to the quark configurations s^4p^2 and s^3p^3 . First, one should take into account their orthogonality to the inner states s^6 and s^5p . According to the results in Sec. III.B and III.C, NN wavefunctions in S and some of P partial waves have a definite nodal structure, which reflects this orthogonality. As it was shown in Refs. [8, 9], such a nodal behavior reproduces an effect of the traditional repulsive core at short NN distances[1)].

To obtain the correct nodal behavior of the NN wavefunction, it is necessary to ensure its orthogonality to the corresponding symmetric $6q$ state, using a projector onto this state, e.g., $P(s^6)$ for the S-wave case. In the space of NN variables, i.e., in the external channel, it reduces to the one-dimensional projection operator P:

$$\langle\psi_N\psi_N|P_{\rm sym}|\psi_N\psi_N\rangle \equiv P = |\phi_0\rangle\langle\phi_0|. \tag{43}$$

1) It should be noted that Neudatchin *et al.* [86, 88, 89] were the first to establish this fact back in the 1970s. In succeeding years, some quantitative attempts were made to confirm this microscopically in terms of a constituent quark model [75, 76] or phenomenologically in terms of the Moscow NN potential [90].

If one uses the harmonic oscillator (h.o.) wavefunctions for the nucleon ($s^3[3]$) and the six-quark ($s^6[6]$) states, the form factor $|\phi_0\rangle$ in the external space is just the nodeless h.o. $|0s\rangle$ state in the *NN* relative-motion variable:

$$|\phi_0\rangle = |0s\rangle_{\text{h.o.}}. \tag{44}$$

Now, to exclude an admixture of the $0s$ function $|\phi_0\rangle$ and to ensure the presence of a stationary node in the external-channel wavefunctions, as required by the microscopic treatment (see, e.g., Eqs. (24) and (26)), the Schrödinger equation (5) for the wavefunction in the external channel should be solved with an additional orthogonality constraint:

$$\langle\Psi^{\text{ex}}|\phi_0\rangle = 0. \tag{45}$$

To solve equations with an additional orthogonality condition, similar to (45), it is convenient to use the orthogonal projection method (see, e.g., [90]). In this method, the equation is solved in full space, but a projector onto the subspace to be excluded [the projector P (43) in our case] with a large coupling constant λ_0 is added to the original Hamiltonian. Thus, we obtain the final form of the effective equation for the external-channel wavefunction:

$$(h^{\text{ex}} + w(E) + \lambda_0 P - E)\Psi^{\text{ex}} = 0. \tag{46}$$

The orthogonalizing term $\lambda_0 P$ in the effective equation (46) replaces the traditional repulsive core in the *NN* interaction. It should be noted that, although the orthogonalizing term $\lambda_0 P$ can be formally assigned to the external channel and included in the external Hamiltonian h^{ex}, its appearance is associated with the six-quark symmetry of the system, i.e., with non-nucleonic degrees of freedom.

A similar situation takes place in P waves. Here the $6q$ wavefunction of the cluster *NN* channel should not contain an admixture of the $s^5p[51]_X$ configuration, which is associated with a quark core. Therefore, passing to the variables of *NN* relative motion, one gets the orthogonality condition:

$$\langle\Psi^{\text{ex}}|\phi_1\rangle = 0, |\phi_1\rangle = |1p\rangle_{\text{h.o.}} \tag{47}$$

and the corresponding projector.

Formally, it is necessary to take a limit $\lambda_0 \to \infty$ to completely exclude the most symmetric $6q$ configurations from the external channel. In practical calculations, it is usually sufficient to take the value of λ_0 to be ca. 10^5 – 10^6 MeV. Note that the admixture of excluded states decreases with increasing λ_0 as λ_0^{-1} . However, keeping in mind that there are no completely forbidden states in the $6q$ system, we can consider a more general case when the admixture of the symmetric component in the wavefunction is not completely excluded, but limited. This can be done using the same projector P in the external channel with a finite value of λ_0 ca. 10^2 – 10^3 MeV. Such a form of interaction is employed below in Sec. V.

C. The results of calculations with the dibaryon (dressed bag) model

The version of the dibaryon model described above, based on the microscopic six-quark description of the *NN* system and referred to as the dressed bag model (DBM) [8, 9], results in the equation (46) with the following effective *NN* interaction:

$$V^{\text{eff}} = v^{\text{ex}} + w(E) + \lambda_0 P. \tag{48}$$

In the DBM, the interaction in the external channel v^{ex} included the one-pion exchange potential (OPEP) with a soft dipole cutoff:

$$v^{\text{OPE}} = -\frac{f_\pi^2}{m_\pi^2}(\boldsymbol{\tau}_1\boldsymbol{\tau}_2)\frac{(\boldsymbol{\sigma}_1\boldsymbol{q})(\boldsymbol{\sigma}_2\boldsymbol{q})}{q^2+m_\pi^2}\left(\frac{\Lambda_{\pi NN}^2 - m_\pi^2}{\Lambda_{\pi NN}^2 + q^2}\right)^2, \tag{49}$$

with $m_\pi = (m_{\pi^0} + 2m_{\pi^\pm})/3$ being the averaged pion mass, $f_\pi^2/(4\pi) = 0.075$ the averaged pion-nucleon coupling constant and $\Lambda_{\pi NN} \simeq 0.6$ – 0.7 GeV/c the high-momentum cutoff parameter, and a small potential v^{TPE} which provided an additional attraction (ca. 2–3 MeV) in the region $r \sim 1.5$ –2 fm:

$$v^{\text{TPE}}(r) = v_0^{\text{TPE}}(\beta r^2)^2\exp(-\beta r^2). \tag{50}$$

In Ref. [9], it was assumed that such a potential could represent the contribution of the peripheral part of the two-pion exchange. This contribution turned out to be important for a precise description of the scattering length and effective radius in the ${}^1S_0$ and ${}^3SD_1$ channels. It should be noted, however, that in the modified version of the dibaryon model generalized to higher partial waves (see Sec. V), the external interaction v^{ex} does not include the terms similar to the potential v^{TPE} .

The model was employed in Ref. [9] for the description of *NN* elastic scattering in the ${}^1S_0$ and ${}^3SD_1$ partial waves and the deuteron properties. A very good description for the elastic scattering data in the energy region from zero to 1 GeV, including the low-energy parameters (scattering length and effective range) and the deuteron static properties such as quadrupole momentum, charge radius and others, was obtained with the weight of the internal (dibaryon) component in the deuteron ca. 3.6%.

In a system of several nucleons, each pair of nucleons can form an intermediate dibaryon state. Consequently, the dibaryon concept inevitably leads to the

emergence of a new three-body force, which arises due to the interaction of a dressed dibaryon formed from a given pair of nucleons with another (third) nucleon. Applying the dibaryon model for NN and $3N$ interactions in a three-nucleon system resulted in a good description of the binding energies for the ^{3}H and ^{3}He nuclei and their Coulomb difference [91–93]. The DBM was also tested in the calculations of the ground states of the ^{6}Li and ^{6}He nuclei [94] within the framework of the three-cluster $\alpha+2N$ model, taking into account a new three-particle force induced by the interaction of the internal dibaryon state with the α core.

Recently, we proposed [13–16] a modified version of the dibaryon model generalized to higher partial waves, which takes into account the presence of experimentally detected dibaryon resonances and allows one to describe both elastic and inelastic NN scattering in a broad energy range well above the pion production threshold. This version of the model is considered in the next Sections.

V. DESCRIPTION OF ELASTIC AND INELASTIC NN SCATTERING

One can make some further simplification of the dibaryon model when the internal space consists of only a single state $|\alpha\rangle$ and the meson degrees of freedom in the internal channel are not considered explicitly [14, 16]. At the same time, the probability of coupling between this state and its possible non-nucleonic decay channels can be taken into account explicitly. In this approximate treatment, the effective interaction $w(E)$ in the external channel has a pole-like energy dependence. However, the pole position has an imaginary part, which corresponds to the possible decays of the internal $6q$ state into inelastic (non-nucleonic) channels. This form of interaction allows one to consider both elastic and inelastic processes in NN scattering. Moreover, this effective interaction leads to the presence of resonances in the whole system, the positions of which can be compared with experimental data. One can expect that such a single-pole approximation for the effective interaction $w(E)$ is justified primarily for the higher NN partial waves where the coupling constants between external and internal channels should be rather small. However, as it has been shown in Ref. [15], the case of strong coupling, which takes place in S waves, can be also considered within this approximation.

Below, we briefly summarize the main results obtained for this version of the model.

A. The effective interaction

With the above simplifications, the external Hamiltonian has the same form as in Eq. (46). It consists of three terms, i.e., the kinetic energy, the OPEP[1)] (49) and the repulsive orthogonalizing potential for some partial waves. Here, the value of λ_0 in the last term remains finite, which corresponds to an incomplete (partial) exclusion of the symmetric $6q$ configuration from the external channel.

The energy-dependent interaction takes a pole-like form:

$$w(E)=\frac{|Z\rangle\langle Z|}{E-E_D}, \tag{51}$$

where E_D is the pole position (see below) and $|Z\rangle$ — the transition form factor which includes the coupling strengths μ. For the uncoupled NN partial waves with a definite value of the orbital momentum L, one has $|Z\rangle=\mu_L|\phi_L\rangle$. For the coupled spin-triplet channels with the total angular momentum J and the tensor coupling of states with orbital momenta $L=J-1$ and $J+1$, we still consider a single state in the internal subspace which, however, couples to both partial external channels. In this case, the transition form factor has the following two-component form: $|Z\rangle\equiv\begin{pmatrix}\mu_{J-1}|\phi_{J-1}\rangle\\ \mu_{J+1}|\phi_{J+1}\rangle\end{pmatrix}$. Thus, for both spin-singlet and spin-triplet NN partial channels, the structure of the interaction potential is the same. The coupling constants from Eq. (42) have a simple pole-like energy dependence:

$$\lambda^J_{SLL'}(E)=\frac{\mu_L\mu_{L'}}{E-E_D}, \tag{52}$$

where the values of the partial strengths μ_L, $\mu_{L'}$ and the energy E_D depend on the total angular momentum J and spin S.

Similarly to the DBM treatment, the form factors $|\phi_0\rangle$ and $|\phi_L\rangle$ are taken as the h.o. functions with the same scale parameter r_0, in accordance to the shell model:

$$\phi_{0L}(k)=A_{0L}(kr_0)^{L+1}\mathrm{e}^{-\frac{1}{2}(kr_0)^2}, \tag{53}$$

$$\phi_L(k)=A_{1L}(kr_0)^{L+1}\left[L+\frac{3}{2}-(kr_0)^2\right]\mathrm{e}^{-\frac{1}{2}(kr_0)^2}, \tag{54}$$

where A_{0L} and A_{1L} are the normalization factors. If the potential contains the orthogonalizing term with the nodeless function (53), then the form factor in the coupling term has the form (54) with *the same* parameter r_0 . If the orthogonalizing term is absent (i.e, $\lambda_0=0$), the coupling form factor is taken in the nodeless form (53).

Thus, in this version of the model, the general form of the interaction remains the same as in the DBM. The

1) In our present calculations, the soft cutoff $\Lambda_{\pi NN}=0.65$ GeV/c is used for all the NN channels except for the $^1S_0$ and coupled $^3SD_1$ configurations where a bit smaller value 0.62 GeV/c is taken [15].

main difference is related to the energy dependence of the coupling constants (42).

B. Account of inelastic processes

For the effective account of inelastic processes and the description of the threshold behavior of the reaction cross section in different partial waves, we may consider the complex-valued energy $E_D = E_0 - \mathrm{i}\Gamma_D/2$, which corresponds to a "bare" dibaryon resonance[1)], and introduce further the energy dependence of the width Γ_D . Here, we assume that inelastic processes occur via the corresponding dibaryon resonance decay. For example, one-pion production goes via the decay modes $D \to \pi NN$ and $D \to \pi d$. The first mode is actually the dominant one for the known isovector dibaryons. In general, the decay widths for both these modes should have similar threshold behaviour, so that, for simplicity, we include just the first one in the Γ_D parametrization and adjust the parameters to effectively take into account the total inelastic width. Thus, we adopt the following representation of Γ_D :

$$\Gamma_D(\sqrt{s}) = \left\{ \begin{array}{ll} 0, & \sqrt{s} \le E_{\rm thr}; \\ \Gamma_0 \dfrac{F(\sqrt{s})}{F(M_0)}, & \sqrt{s} > E_{\rm thr} \end{array} \right\}, \qquad (55)$$

where $\sqrt{s}$ is the total invariant energy of the decaying resonance, M_0 — the "bare" dibaryon mass, $E_{\rm thr} = 2m + m_\pi$ — the threshold energy, and Γ_0 defines the decay width at the resonance energy.

The function $F(\sqrt{s})$ should take into account the dibaryon decay into the πNN channel. Therefore, for the given values of the orbital angular momenta of the pion l_π and NN pair L_{NN}, this function can be parameterized as follows:

$$F(\sqrt{s}) = \frac{1}{s}\int_{2m}^{\sqrt{s}-m_\pi} \mathrm{d}M_{NN} \frac{q^{2l_\pi+1}k^{2L_{NN}+1}}{(q^2+\Lambda^2)^{l_\pi+1}(k^2+\Lambda^2)^{L_{NN}+1}}, \quad (56)$$

where $q = \sqrt{(s - m_\pi^2 - M_{NN}^2)^2 - 4m_\pi^2 M_{NN}^2}\big/2\sqrt{s}$ is the pion momentum in the total c.m.s., $k = \frac{1}{2}\sqrt{M_{NN}^2 - 4m^2}$ — the momentum of the nucleon in the c.m.s. of the final NN subsystem with the invariant mass M_{NN}, and Λ — the high-momentum cutoff parameter, which prevents an unphysical rise of the width Γ_D at high energies. The orbital momenta l_π and L_{NN} may take different values, whereas their sum is restricted by the total angular momentum and parity conservation.

In the isoscalar channels, the main inelastic process is the two-pion production. In this case, one may use Eq. (55) and an expression for $F(\sqrt{s})$ similar to Eq. (56) but for the $D \to \pi\pi d$ decay [14].

The separable form of the interaction (51) allows one to find the resonance parameters straightforwardly. In this case, the explicit expressions for the S-matrix and inelastic cross section can be written. The latter has a similar form to the Breit–Wigner (BW) one. However, it contains an additional energy dependence in both terms of the BW denominator. Thus, the resulting energy-dependent width consists of the initial "bare" width Γ_D and a term which results from the coupling with the external NN channel. The resonance position shifts due to this coupling as well (see details in Refs. [13] and [14]). Thus, in this version of the model, the coupling between the external NN and the internal ("bare" dibaryon) channels leads to a renormalization of the complex energy of the initial "bare" dibaryon and its transformation to the physical mass and width of the "dressed" dibaryon, which can be deduced from experimental data.

C. Elastic and inelastic NN scattering amplitudes

The results for particular NN partial-wave amplitudes have been reported in Refs. [13–16]. Here we summarize the results for the lowest 14 NN partial channels, including new and updated fits for some channels, which have not been considered previously. We use the conventional K-matrix notations [24, 25] for the partial phase shifts, inelasticity parameters and mixing angles.

1. *Channels related to the known dibaryon resonances*

We start from 10 NN channels (including three coupled-channel configurations), where experimental evidences for the corresponding 7 dibaryon resonances take place (see Sec. II). The model parameters for these channels are collected in Table 1. The data for the channels with definite values of J are separated by lines. The parameter values have been fitted to reproduce the partial phase shifts and inelasticities in each partial configuration. Thus, we obtained the "bare" masses M_0 to be rather close to the masses of the known dibaryon resonances which, in turn, are close to the respective di-hadron thresholds ($N\Delta$, $NN^*(1440)$ or $\Delta\Delta$), as discussed in Sec. II.A.3. The values of λ_0 reflect the repulsive part of the interaction, which is also consistent with the nodal structure of the corresponding wavefunctions (see Sec. III.C). The values of r_0 should depend on the features of the internal state as well. In fact, r_0 changes not so arbitrary as it may seem from Table 1. As it has been noted above, we use different form factors given by Eqs. (53) and (54), i.e., represented by the nodeless h.o. function (when $\lambda_0 = 0$) and the h.o. function with one node (when $\lambda_0 \neq 0$), respectively. The effective ranges $R = \sqrt{\langle r^2 \rangle}$ of the above h.o. functions are different and additionally de-

1) Actually, we mean here a $6q$ state dressed with meson loops, but not with the NN loops.

Table 1. The dibaryon model parameters for the lowest NN partial channels.

$^{2S+1}L_J$	λ_0/MeV	r_0/fm	μ_L/MeV	M_0/MeV
$^1S_0$	165	0.48	274.2	2300.313
$^3S_1$	165	0.475	248.1	2275.69
$^3D_1$	0	0.6	65.9	
$^3P_0$	450	0.425	35	2200
$^3P_2$	0	0.7	65	2205
$^3F_2$	105	0.45	1.5	
$^1D_2$	0	0.82	48	2168
$^3D_3$	0	0.71	58	2363
$^3G_3$	0	0.71	36	
$^3F_3$	0	0.5	70	2240

pend on the orbital momentum value L. Thus, $R = r_0\sqrt{L+3/2}$ for the nodeless function and $R = r_0\sqrt{L+7/2}$ for the h.o. function with one node. Taking into account these effective ranges, one can find that the smallest $R \approx 0.9$ fm corresponds to the S waves and $^3P_0$ wave, and the value of R rises for higher partial waves, which looks reasonable[1)].

In Fig. 3, the partial phase shifts, mixing angles and inelasticity parameters for the coupled spin-triplet channels $^3S_1 - {}^3D_1$, $^3P_2 - {}^3F_2$ and $^3D_3 - {}^3G_3$ are shown in comparison with the single-energy and energy-dependent solutions of the SAID PWA [35, 36, 58]. We compare all our results with the SAID solution SM16 [58], except for the $^3D_3 - {}^3G_3$ channels, where we use for comparison the solution AD14 [35, 36], which gives an S-matrix pole corresponding to the $d^*(2380)$ dibaryon resonance. The partial phase shifts for the rest uncoupled channels $^1S_0$, $^3P_0$, $^1D_2$ and $^3F_3$ are presented in Fig. 4.

A good agreement can be noticed between the dibaryon model predictions and the SAID PWA solutions up to rather high laboratory energies $T_{\rm lab}$, which correspond to the resonance position in each case. For the coupled-channel configurations, some discrepancies are seen for the $^3G_3$ phase shift and mixing angle ϵ_3, which require a further improvement of the model. At the same time, the coupled NN channels $^3D_3 - {}^3G_3$ correspond to the most evident case, for which the resonance-like behavior of the NN elastic scattering amplitudes (due to the dibaryon state d^* (2380)) has been found experimentally and confirmed by the SAID PWA as well [35–37].

Our model description of the NN scattering amplitudes also takes into account inelastic processes. For the majority of partial channels, the parametrization (55) for the imaginary part of the internal-state energy E_D with a decay width in the form of Eq. (56) corresponding to the $D \to \pi NN$ decay has been used. The respective parameter values are listed in Table 2. Here, the values of Γ_0 differ evidently which is caused particularly by a strong dependence of the pion production probability on the NN channel quantum numbers. The available parameters l_π and L_{NN} are restricted by the parity and total angular momentum conservation, and their particular values, as well as the cut-off parameter Λ, have been adjusted to get the best fit of the SAID single-energy data for the inelasticity ρ in the near-threshold region. The large spread of the Λ values highlights the need for a more accurate treatment of the dibaryon width in some partial channels. In particular, a very slow rise of the $^3S_1$ inelasticity from threshold is related to the low single-pion production probability and importance of the two-pion decay mode

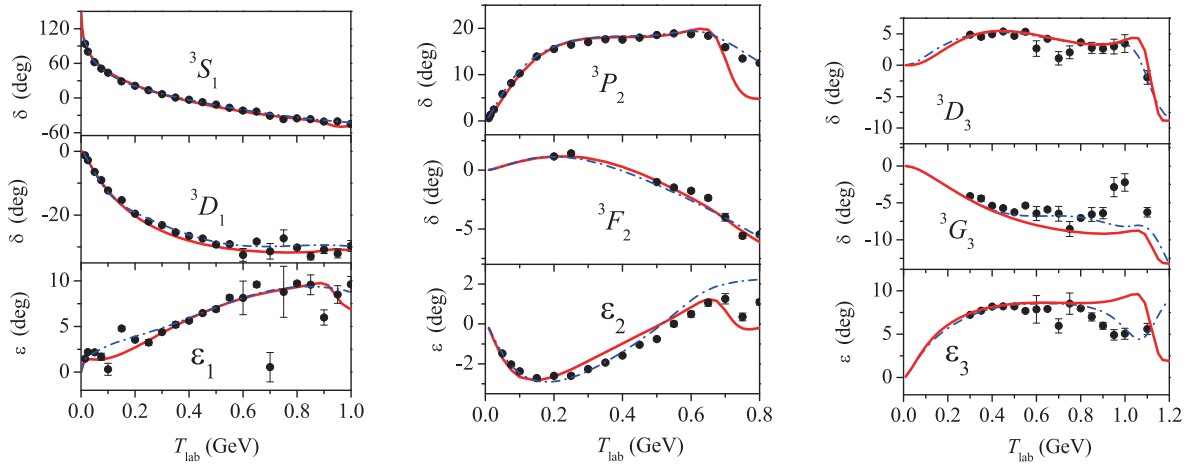

Fig. 3. (color online) Phase shifts and mixing angles for the coupled NN partial channels found within the dibaryon model (solid curves) in comparison with the SAID PWA single-energy (circles) and energy-dependent (dash-dotted curves) solutions: SM16 [58] for the $^3S_1$–$^3D_1$ and $^3P_2$–$^3F_2$ channels and AD14 [35, 36] for the $^3D_3$–$^3G_3$ channels.

1) A more detailed analysis of the model parameters will be given in the forthcoming study.

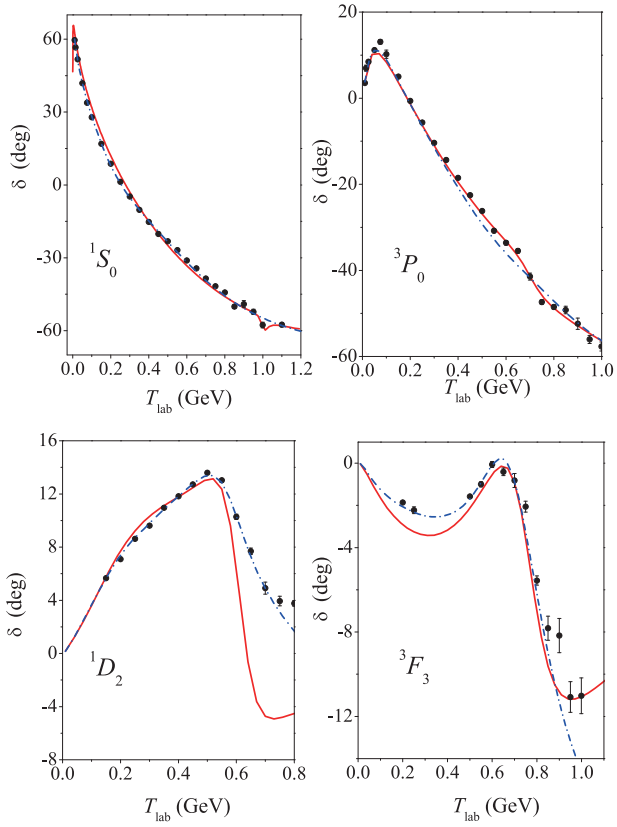

Fig. 4. (color online) Phase shifts for the uncoupled NN partial channels $^1S_0$, $^3P_0$, $^1D_2$ and $^3F_3$ found within the dibaryon model (solid curves) in comparison with the SAID PWA single-energy (circles) and energy-dependent SM16 (dash-dotted curves) solutions [58].

Table 2. Parameters used for the representation of Γ_D (see Eqs. (55) and (56)) in the lowest NN partial channels.

$^{2S+1}L_J$	Γ_0/MeV	Λ/MeV	l_{NN}	l_π
$^1S_0$	40	300	0	1
$^3SD_1$	80	1800	2	1
$^3P_0$	92	87	0	0
$^3PF_2$	100	1000	0	2
$^1D_2$	100	300	1	0
$^3F_3$	150	100	2	0

in this channel. Since we focus here on the general description of NN data in a wide energy range, we postpone the refinement of the model for a better description of the near-threshold behavior of some partial amplitudes to a future work.

For the coupled channels $^3DG_3$, the dibaryon width (55) should include predominantly the two-pion decay mode, which gives the main impact to the inelasticity here. Thus, we used here the parametrization of the decay width similar to Eq. (56) but for the $D \to d\pi\pi$ decay, with the following parameters: $\Gamma_0 = 60$ MeV, $l_d = l_{\pi\pi} = 1$, $\Lambda = 150$ MeV (see details in Ref. [14]).

Table 3. Parameters ($M_{\rm th}$, $\Gamma_{\rm th}$) of the dressed dibaryons (in GeV) found in the present model for seven NN configurations and their empirical values from the references given in the last column.

$^{2S+1}L_J$	$T(J^P)$	$M_{\rm th}$	$\Gamma_{\rm th}$	$M_{\rm exp}$	$\Gamma_{\rm exp}$	Ref.
$^1D_2$	$1(2^+)$	2.18	0.14	2.14–2.18	0.05–0.11	[21–23, 62]
$^3P_0$	$1(0^-)$	2.2	0.1	2.201(5)	0.091(12)	[59]
$^3PF_2$	$1(2^-)$	2.221	0.17	2.197(8)	0.130(21)	[59]
$^3F_3$	$1(3^-)$	2.23	0.185	2.20–2.26	0.1–0.2	[20, 62]
$^3SD_1$	$0(1^+)$	2.31	0.16	2.315(10)	0.150(30)	[15]
$^1S_0$	$1(0^+)$	2.33	0.05	2.32	0.15	[15]
$^3DG_3$	$0(3^+)$	2.376	0.084	2.38(1)	0.08(1)	[35,36]

The comparison of inelasticity parameters ρ with the SAID PWA data for the majority of the NN partial channels is shown in Fig. 5. For the visual representation, the dependence of the data on the total invariant energy $\sqrt{s}$ is used here. Except for the $^3D_1$ partial wave, all figures reflect good agreement of the model calculations with the PWA data up to the invariant energy values corresponding to the pole position. At higher energies, the calculated inelasticities decrease, while the PWA data still grow up. This behavior has been expected, because we employ the resonance-like parametrization for the decay width. Other inelastic processes not included into our model treatment should also give impact to the total inelastic amplitudes at higher energies.

Finally, in Table 3, the dressed dibaryon resonance parameters found from our model fits are compared with the parameters obtained by PWA or phenomenological analysis from the experimental data[1)]. The raws of the Table are sorted by the increasing resonance masses. Nearly all the dibaryon parameters occur to be in quite reasonable agreement with the empirical values quoted in the last column of the Table. The resulting shift of the dressed dibaryon mass $M_{\rm th}$ with regard to the initial value M_0 given in Table 1 for each partial configuration is caused by the coupling between the internal and external (NN) channels and depends on the coupling strength μ_L, the type of the form factor and the external part of the NN interaction (see details in Refs. [13, 14]).

The results presented in Figs. 3–5 show that the pole-like form of the interaction leads to a rather good description of the NN partial channels with an evident repulsion. In particular, the phase shifts are reproduced quite well, even at energies above the resonance positions, though the inelasticities have the wrong decreasing there. At the

1) The "trivial" dibaryons in the $^3SD_1$ (the deuteron) and $^1S_0$ (the singlet deuteron) partial channels are not included here.

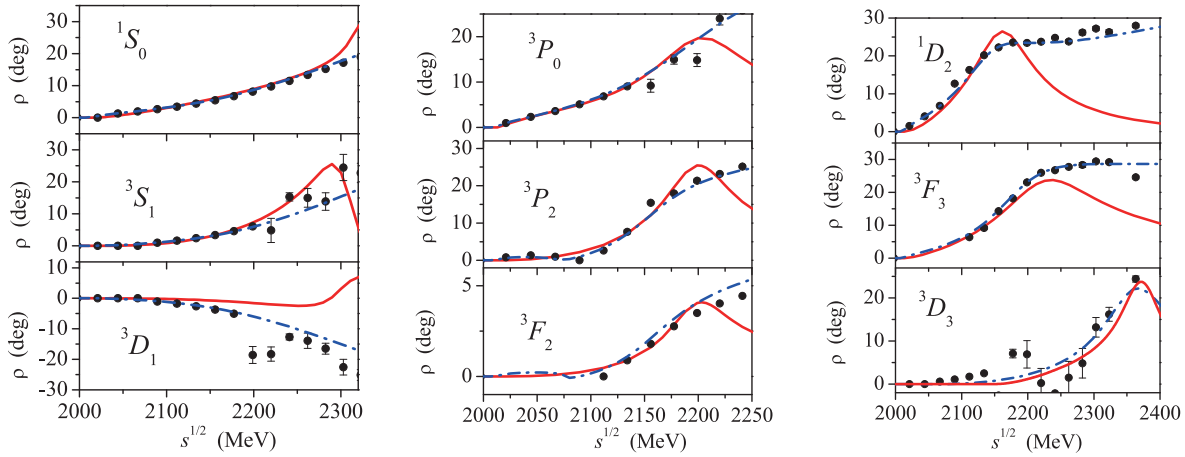

Fig. 5. (color online) Inelasticity parameters for the coupled and uncoupled *NN* partial channels found within the dibaryon model (solid curves) in comparison with the SAID PWA single-energy (circles) and energy-dependent (dash-dotted curves) solutions [35, 36, 58].

same time, for the channels without repulsion, such as $^1D_2$, $^3P_2$ and $^3DG_3$, the phase shifts are described properly up to the resonance energies only. This behavior is directly related to the decrease of inelasticities. Thus, some refinement of the model is required if one needs to move to the higher energy region. This could be done by an inclusion of other possible inelastic processes, account for the dynamics in the internal channel, etc.

In summary, we have achieved a very good quantitative description for the partial phase shifts in the *NN* channels considered and a rather good qualitative description for the inelasticity parameters in a broad energy range starting from zero energy which is very far from the position of the "bare" dibaryon. The very important feature of the results presented above is good agreement of the masses and widths of the dressed dibaryons obtained by fitting the *NN* phase shifts and inelasticities in our model with the dibaryon parameters deduced from experiments.

The success of the model for the *NN* channels with the known dibaryon resonances allows us to make a step forward and extend the suggested model for partial channels, where the existence of dibaryon resonances is not confirmed to date.

2. *Partial NN channels for which dibaryon states have not been found yet*

Below, we discuss the uncoupled *NN* partial channels where the dibaryon resonances have not been reliably detected to date. These are the isovector channel $^3P_1$ and three isoscalar channels $^1P_1$, $^3D_2$ and $^1F_3$.

For some of the *NN* channels in question, indications of possible resonances exist in the literature. In particular, the $^3P_1$ resonance was found in the PWA [26, 27]. In Ref. [16], we have constructed the dibaryon potential for the $^3P_1$ channel [16], where the resonance with a position rather close to those for the $^3P_0$ and $^3P_2$ channels has been predicted. For the isoscalar *NN* channel $^1P_1$, the estimations can be done [66] based on the resonance-like behavior of the isoscalar part of the *NN*-induced single-pion production near the $NN^*(1440)$ threshold [15, 65]. At the same time, we are not aware of any indications of the dibaryon resonances in the channels $^3D_2$ and $^1F_3$.

The dibaryon model parameters used for fitting the partial phase shifts in the above *NN* channels are collected in Table 4. Here, the values of the parameters M_0 and r_0 for the channel $^3P_1$ happened to be rather close to those for the channel $^3P_0$ (see Table 1), while for other three (isoscalar) channels, they are comparable to the values for the $^3S_1$ channel.

We have also fitted the inelasticity parameters for the partial channels $^3P_1$ and $^1P_1$. The internal state width has been parameterized by Eqs. (55) and (56). The respective parameters are given in Table 5. We have not

Table 4. Dibaryon model parameters for the *NN* partial channels $^1P_1$, $^3P_1$, $^3D_2$ and $^1F_3$.

$^{2S+1}L_J$	λ_0/MeV	r_0/fm	μ_L/MeV	M_0/MeV
$^3P_1$	270	0.425	20	2230
$^1P_1$	280	0.48	90	2320
$^3D_2$	120	0.5	165	2350
$^1F_3$	120	0.51	70	2345

Table 5. Same as in Table 2 for the partial channels $^3P_1$ and $^1P_1$.

$^{2S+1}L_J$	Γ_0/MeV	Λ/MeV	l_{NN}	l_π
$^3P_1$	50	200	0	0
$^1P_1$	110	300	1	1

considered the inelasticities in the $^3D_2$ and $^1F_3$ partial waves, since they are missing in the SAID PWA. For these partial channels, the invariant mass of the resonance can be definitely found, while the width cannot be solely estimated from the fit of elastic phase shifts. At the same time, the model potential for these channels has a repulsive part. Thus, the decay widths of the internal states contribute to the phase shifts in the narrow region near the resonance position only.

The comparison of the calculated partial phase shifts with the SAID PWA solutions for the above NN channels is shown in Fig. 6.

The inelasticity parameters for the P-wave channels are presented in Fig. 7. A good agreement of our model calculations with the PWA data is observed.

Our theoretical calculations within the dibaryon model predict two resonances in the NN partial channels $^3P_1$ and $^1P_1$ with the quantum numbers $T(J^P) = 1(1^-)$ and $0(1^-)$, respectively, and the following parameters: $M_{\rm th}(^3P_1) =$ 2.23 GeV, $\Gamma_{\rm th}(^3P_1) =$ 0.05 GeV and $M_{\rm th}(^1P_1) = 2.33$ GeV, $\Gamma_{\rm th}(^1P_1) = 0.13$ GeV. We have also predicted two more isoscalar states with the masses close to 2.35 GeV in the NN channels $^3D_2$ and $^1F_3$, however, their widths could not be defined accurately.

From the results presented in Table 3 and this subsection, one may conclude that dibaryon states can be divided into two groups according to their masses. The majority of the isovector states (except for the $^1S_0$ one) lie near the $N\Delta$ threshold, while the masses of the isoscalar states (and the $^1S_0$ state as well) are close to the NN^* (1440) and $\Delta\Delta$ thresholds. These findings should correspond to the internal structure of the six-quark systems with different isospins. It seems likely that such a dibaryon $|DB\rangle$ can be represented as a mixed state of the six-quark core and the hadron molecule (a loosely bound $N+N^*$ state), $|DB\rangle = \cos\theta|6q\rangle + \sin\theta|NN^*\rangle$, where θ is the mixing angle. Recently, such an approach has been successfully used in the baryon sector for the description of the Roper resonance represented as $|R\rangle = \cos\theta_r|3q\rangle + \sin\theta_r|N\sigma\rangle$ [95, 96]. The molecular $N\sigma$ component plays a role for the understanding of both the helicity amplitudes of the Roper resonance electroproduction and a large 2π branching in this reaction. In the case of the DB, there is a good probability that the hadronic molecular mode NN^*, when present, will be also seen in the pion electroproduction off the deuteron at large momentum transfer or in the pion photoproduction near the NN^* threshold[1)].

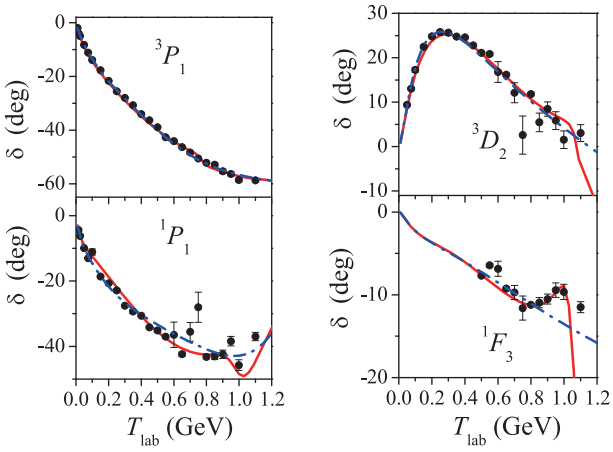

Fig. 6. (color online) Partial phase shifts for the NN channels $^1P_1$, $^3P_1$, $^3D_2$ and $^1F_3$ found within the dibaryon model (solid curves) in comparison with the SAID PWA single-energy (circles) and energy-dependent SM16 (dash-dotted curves) solutions [58].

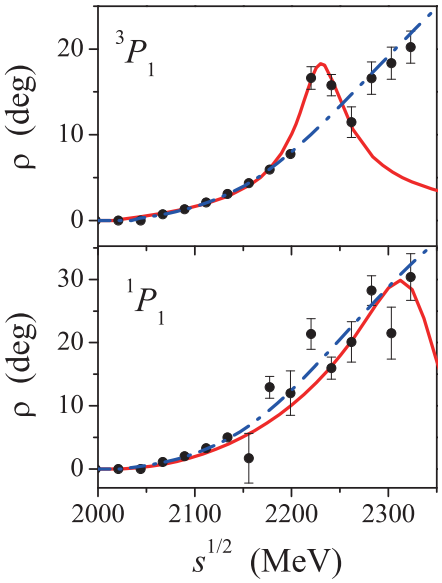

Fig. 7. (color online) Inelasticity parameters for the NN partial channels $^1P_1$ and $^3P_1$ found within the dibaryon model (solid curves) in comparison with the SAID PWA single-energy (circles) and energy-dependent SM16 (dash-dotted curves) solutions [58].

VI. CONCLUSION

In this study, we presented the new QCD-motivated approach to NN scattering at intermediate energies — the dibaryon model, which includes the dibaryon resonance formation at short NN distances supplemented by the peripheral one-pion-exchange at long distances. This novel approach implements the duality principle for NN scattering (see, e.g., [10]), i.e., it replaces the t-channel multimeson exchanges in the traditional NN-potential models by the s-channel mechanism corresponding to the exchange of the dibaryon resonance (the $6q$ bag dressed with meson fields) between the interacting nucleons in their overlap region. We argued that dibaryon resonances

1) The NN^* mode should contain also the $NN\sigma$ (or dibaryon+σ) component in the case when N^* is the Roper resonance.

can serve as a bridge between the traditional picture of the *NN* interaction dealing with point-like nucleons and mesons and the QCD world dealing with quarks and gluons. Based on the microscopic six-quark consideration of the *NN* system, we have shown that the dibaryon degrees of freedom are appropriate to effectively take into account the inner structure of the nucleons in the *NN* scattering processes.

The purpose of this work was not to prove the existence of dibaryon resonances. Instead, we employed their parameters deduced from analysis of the recent experiments [4, 5] to build some alternative picture of the short-range *NN* interaction. We have demonstrated that the simple two-channel model including a single dibaryon pole in the internal channel is able to describe reasonably well the *NN* scattering phase shifts and inelasticity parameters in all basic (*S*, *P*, *D*, *F*) partial waves in a broad energy range from zero up to 0.7–1.2 GeV using a few adjustable parameters in each partial wave. One should note in this respect that the high-precision *NN* potentials based on the traditional meson-exchange picture as well as the state-of-the-art *NN* potential derived within the chiral perturbation theory describe very well the elastic phase shifts up to 350 MeV and are not intended for reproducing the inelasticities. Though we employed the phenomenological determination of the model parameters in the present work, we have shown that these parameters can in principle be obtained from the six-quark microscopic treatment for the *NN* system. An important result of the present study is that the dibaryon resonance parameters, found from our model fit to the phase shifts, turned out to be in good agreement with the empirical values.

Thus, we have found the direct connection between the observable properties (masses, widths, decay modes) of dibaryons detected to date and observables of *NN* elastic and inelastic scattering. The next steps along this way would be the calculations of the properties of few-body systems, finite nuclei, and nuclear matter starting from the *NN* and 3*N* interactions derived within the dibaryon model.

We have also predicted a few dibaryon resonances in the partial waves, where they have not been found yet. This result stimulates further experimental research of *NN* observables at intermediate energies. Thus, the new data on the sensitive spin-dependent observables could help refine the current *NN* PWA solutions and reveal new dibaryon states. Still the main information on dibaryon resonances has been obtained from the inelastic processes involving the two-nucleon system. The experimental studies of photoproduction of mesons on the deuteron and deuteron photodisintegration recently undertaken and planned at, e.g., MAMI [38, 39] and ELPH [67–69] seem to be very promising in exploring the properties of the known dibaryons as well as in finding the new ones. In view of the recent experimental progress in the field, one can say that we stand at the beginning of dibaryon spectroscopy.

The results of the present work support our claim that the six-quark states are not just exotic hadrons like tetra- or pentaquarks, but a regular mode in the fundamental *NN* interaction carrying the basic intermediate-range attraction and also responsible for the short-range repulsion between nucleons. Thus, the dibaryon model can be considered as a new QCD-motivated tool appropriate for an effective treatment of the short-range nuclear force, since it is free of some limitations of both quark and meson-exchange models and therefore has a wider range of applicability. These findings make further research of dibaryon resonances very perspective. It would be also interesting to study the connection between the *s*-channel mechanism suggested in this work and the contact terms used in the chiral perturbation theory.

APPENDIX A: PARAMETRIZATION OF THE TRANSITION AMPLITUDE ON THE BASIS OF THE DRESSED BAG MODEL

In the dressed bag model [8, 9], the transition from the internal ($6q+\sigma$) channel to the external (NN) channel is described in terms of the RGM ansatz (8). In line with Eq. (12), the transition matrix element can be written as:

$$h^{\rm ex,in}|\alpha,\boldsymbol{k}\rangle \to \langle\{NN\}^{\mathcal{Q}}|\mathcal{A}h^{\rm ex,in}_{6q}|\alpha,\boldsymbol{k}\rangle = \langle\{NN\}^{\mathcal{Q}}|\hat{O}_{\sigma}|\alpha,\boldsymbol{k}\rangle, \tag{A1}$$

where $[NN]^{\mathcal{Q}}$ is an external *NN* state orthogonalized to the $6q$ configuration $s^6[6]_X$ (for a positive parity) or $s^5p[51]_X$ (for a negative parity):

$$|\{NN\}^{\mathcal{Q}}\rangle = \Gamma^{\mathcal{Q}}|\{NN\}\rangle, \tag{A2}$$

where

$$\Gamma^{\mathcal{Q}} = \left\{ \begin{matrix} I-|\Psi_0\rangle\langle\Psi_0|, \text{ for } S \text{ wave}, \\ I-|\Psi_1\rangle\langle\Psi_1|, \text{ for } P \text{ wave}, \end{matrix} \right\} \tag{A3}$$

and $\hat{O}_{\sigma}$ is some operator of the σ-meson annihilation (vertex *B* in Fig. 2). Note that the operator of antisymmetrization $\mathcal{A} = \frac{1}{10}(I - \sum_{i=1}^{3}\sum_{j=4}^{6} P_{ij})$ is omitted in the r.h.s. of Eq. (A1), since, by definition, both the s^6 and s^5p components of the dressed bag (i.e., the configurations Ψ_0 and Ψ_1) are antisymmetric under quark permutations [see, e.g., Eq. (25)].

It is important that the projection operator $\Gamma^{\mathcal{Q}}$, defined in Eq. (A3), may be represented in terms of the excited

$6q$ configurations s^4p^2 or s^3p^3, i.e., in terms of the wavefunctions $\Psi_n^{(i)}$ defined by Eqs. (16), (18) or (22), (23), respectively. All one has to do is to construct the cluster $3q+3q$ state with the quantum numbers of the *NN* channel on the basis of the shell-model wavefunctions $\Psi_n^{(i)}$:

$$|Q_n^{NN}\rangle = \sum_i U_{ni}^{NN}|\Psi_n^{(i)}\rangle. \tag{A4}$$

Here, $Q_n^{NN}(\boldsymbol{r},\{\boldsymbol{\rho}\boldsymbol{\xi}\})$ denotes the wavefunction of the cluster ($3q$+$3q$) state at short distances and U_{ni}^{NN} are the fractional parentage coefficients (f.p.c.) [83–85] for separation of two nucleonic $3q$ clusters in the $6q$ configurations $\Psi_n^{(i)}$. For example, the *NN* cluster state in the configuration s^4p^2 with $ST=10$ (the $^3S_1$ partial wave) looks like:

$$\begin{aligned}|Q_2^{NN},ST=10\rangle =& -\sqrt{\frac{9}{20}}\Psi_2^{(1)}+\sqrt{\frac{16}{45}}\Psi_2^{(2)}\\ &+\sqrt{\frac{1}{36}}\Psi_2^{(3)}-\sqrt{\frac{1}{18}}\Psi_2^{(4)},\end{aligned} \tag{A5}$$

where the coefficients are from the first row of Table A1, which lists the $6q\to 3q+3q$ f.p.c.'s for the configuration $s^4p^2[42]_X(ST=10)$. The values of U_{ni}^{NN} are defined as the amplitudes for the overlapping of the CST parts of the $6q$ and $3q$+$3q$ wavefunctions:

$$U_{ni}^{NN}(CST)=\langle N(C_1S_1T_1)N(C_2S_2T_2)|\Psi_n^{(i)}(CST)\rangle,$$

where $|N(CST)\rangle$ is given in Eq. (13) and $|\Psi_n^{(i)}(CST)\rangle$ can be taken from Eq. (16). A special advantage of using the coefficients $U_{ni}^{NN}(CST)$ is that they are independent of dynamics and are calculated by the group theoretical methods [83, 86].

Table A1. Baryon-baryon (B_1B_2) content of the $6q$ configuration $s^4p^2[42]_X[f_i]_{CS}ST=10$ (i=0, 1, ... 5) represented by the f.p.c.'s $U_{2i}^{B_1B_2}$. The notation $U_{2i}([42]_X)$ is used for the coefficients $U_{2i}^{B_1B_2}$ which appear in Eqs. (A4)–(A7) for $B_1B_2=NN$.

	$U_{20}([6]_X)$	$U_{2i}([42]_X)$				
$B_1B_2\backslash i$	$[2^3]_{CS}$	$[42]_{CS}$	$[321]_{CS}$	$[2^3]_{CS}$	$[31^3]_{CS}$	$[21^4]_{CS}$
	0	1	2	3	4	5
NN	$\sqrt{\frac{1}{9}}$	$-\sqrt{\frac{9}{20}}$	$\sqrt{\frac{16}{45}}$	$\sqrt{\frac{1}{36}}$	$-\sqrt{\frac{1}{18}}$	0
$\Delta\Delta$	$-\sqrt{\frac{4}{45}}$	0	0	$\sqrt{\frac{16}{45}}$	0	$\sqrt{\frac{5}{9}}$
C_1C_1	$\sqrt{\frac{2}{9}}$	$-\sqrt{\frac{1}{10}}$	$-\sqrt{\frac{8}{45}}$	$\sqrt{\frac{1}{18}}$	$\sqrt{\frac{4}{9}}$	0
C_1C_2	$\sqrt{\frac{4}{9}}$	$\sqrt{\frac{1}{5}}$	$-\sqrt{\frac{1}{45}}$	$\sqrt{\frac{1}{9}}$	$-\sqrt{\frac{2}{9}}$	0
C_2C_2	$\sqrt{\frac{1}{45}}$	$\sqrt{\frac{1}{4}}$	$\sqrt{\frac{4}{9}}$	$\sqrt{\frac{1}{180}}$	$\sqrt{\frac{5}{18}}$	0
C_3C_3	$-\sqrt{\frac{1}{9}}$	0	0	$\sqrt{\frac{4}{9}}$	0	$-\sqrt{\frac{4}{9}}$

With the cluster *NN* state defined by Eq. (A4), one may represent the projection operator (A2) in the form

$$\Gamma^{Q}=|Q_n^{NN}\rangle\langle Q_n^{NN}|+\ldots, \tag{A6}$$

where dots symbolize terms of little importance at short range. Then the transition matrix element (A1) takes the form:

$$\begin{aligned}h^{\rm ex,in}|\alpha,\boldsymbol{k}\rangle =&\langle\{NN\}^{Q}|\hat{O}_\sigma|\alpha,\boldsymbol{k}\rangle\\ =&\langle\{NN\}|\sum_i U_{ni}^{NN}|\Psi_n^{(i)}\rangle\sum_j U_{nj}^{NN}\langle\Psi_n^{(j)}|\hat{O}_\sigma|\alpha,\boldsymbol{k}\rangle,\end{aligned} \tag{A7}$$

and thus, both the form factor $Z_{LS}^{JM}(r)$ and vertex function $B_{L_\alpha LS}^{J}(k,E)$ introduced in Eq. (39) (see Sec. IV.A) obtain a microscopic interpretation in terms of Eq. (A7):

$$Z_n(\boldsymbol{r})=\sum_i U_{ni}^{NN}\langle\{NN\}_{ST}|\Psi_n^{(i)}\rangle, \tag{A8}$$

$$B_n(\boldsymbol{k},E)=\sum_j U_{nj}^{NN}\langle\Psi_n^{(j)}|\hat{O}_\sigma(\boldsymbol{k},E)|\alpha,\boldsymbol{k}\rangle. \tag{A9}$$

After a partial-wave decomposition of the r.h.s. of Eqs. (A7)–(A9), the functions Z_n and B_n transform into $Z_{LS}^{JM}(r)$ and $B_{L_\alpha LS}^{J}(k,E)$, respectively, and Eq. (A7) becomes equivalent to Eq. (39).

It is important that the quark model restricts the form of the overlap functions $\langle\{NN\}|\Psi_n^{(i)}\rangle$ in the r.h.s. of Eq. (A8), as is seen from the comparison of these functions with those defined in Eqs. (27) and (31). For example, keeping in mind that at $n=2(3)$ the values of LST should be fixed at $L=0(1)$, $ST=10,01(11,00)$, one obtains the following expression for the partial wave decomposition of the form factor (A8):

$$\begin{aligned}Z_{LS}^{JM}(r)=&\sum_i U_{ni}^{NN}\left\{\int Y_L^*(\hat{r})d\Omega_r\langle\{NN\}_{ST}|\Psi_n^{(i)}\rangle\right\}_{JM}\\ =&\begin{cases}\mathcal{N}_n\left(1-\dfrac{r^2}{b^2}\right)\exp\left(-\dfrac{3r^2}{4b^2}\right), n=2,\\ \mathcal{N}_n r\left(1-\dfrac{r^2}{b^2}\right)\exp\left(-\dfrac{3r^2}{4b^2}\right), n=3,\end{cases}\end{aligned} \tag{A10}$$

where the normalization factors $\mathcal{N}_n, n=2,3$ should take

into account the contributions of both the coefficients U_{ni}^{NN} and the overlap integrals over the inner nucleonic coordinates $\{\boldsymbol{\rho}\boldsymbol{\xi}\}$. Note that the integration over Ω_r in Eq. (A10) is formal here, since the value of L is already fixed by the given value of n.

The quark model also restricts the form of the vertex functions $B^J_{L_\sigma LS}(k)$. As is evident from Eq. (A9), the functions $B_n(\boldsymbol{k},E)$ should be proportional to the shell-model matrix elements $\langle\Psi_n^{(j)}|\hat{O}_\sigma(\boldsymbol{k},E)|\Psi_m\rangle$, $m=0,1$, where Ψ_m means the $6q$ component of the dressed bag state $|\alpha,\boldsymbol{k}\rangle$ [8, 9]. The corresponding wavefunctions are given in Eqs. (14)–(15) (for a positive parity) and (20)–(21) (for a negative parity). The partial wave decomposition of $B_n(\boldsymbol{k},E)$ is analogues to Eq. (A10), corrected for the substitution of $\langle\Psi_n^{(j)}|\hat{O}_\sigma(\boldsymbol{k},E)|\Psi_m\rangle$ for $\langle\{NN\}_{ST}|\Psi_n^{(i)}\rangle$ (see Appendix B for the calculation of the shell-model matrix element $\langle\Psi_n^{(j)}|\hat{O}_\sigma(\boldsymbol{k},E)|\Psi_m\rangle$).

APPENDIX B: QUARK-MODEL CALCULATION OF THE TRANSITION AMPLITUDE

The vertex functions $B^J_{L_\sigma LS}(k,E)$ determining the transition from the external NN to the internal $(6q+\sigma)$ channel were calculated in Refs. [8, 9] for the lowest even partial waves (L = 0,2), assuming the emission of the s-wave σ meson (L_σ= 0) from the initial $|s^4p^2[42]_X\rangle$ six-quark state. The calculations were performed within the framework of TISM including all $6q$ configurations with 0 $\hbar\omega$, 1 $\hbar\omega$ and 2 $\hbar\omega$ excitations, subsequently denoted as d_0, $d_1'(d_1'')$ and d_2 . For this, the two-pion emission amplitude in the transition from the orthogonalized [in a sense of Eq. (45)] NN state to the dressed $6q$ bag $d_0+\sigma(2\pi)$ was calculated. The graph illustrating this process is shown in Fig. B1.

The transition goes in two steps via intermediate $6q$ states $d_1'(d_1'')$:

$$[NN]^Q \to d_1'(d_1'')+\pi \to d_0+\sigma(2\pi) \qquad \text{(B1)}$$

(for the even partial waves L = 0, 2 in the initial NN state). The final $6q$ state in Fig. B1 is the most symmetric (and compact) shell-model quark configuration $d_0 = s^6[6]_X$. The intermediate six-quark states d_1' (d_1'') denoted by the vertical dashed line in the graph belong to the configurations $s^5p[51]_X[f]_{CS}(ST)$ and have the following quantum numbers: $d_1'(ST=10, J^P=0^-)$ for the singlet NN channel[1)] and $d_1''(ST=01, J^P=1^-)$ for the triplet channel.

Here we briefly outline the scheme for calculating the amplitude (B1) with the successive emission of two pions shown in Fig. B1. The amplitude can be represented

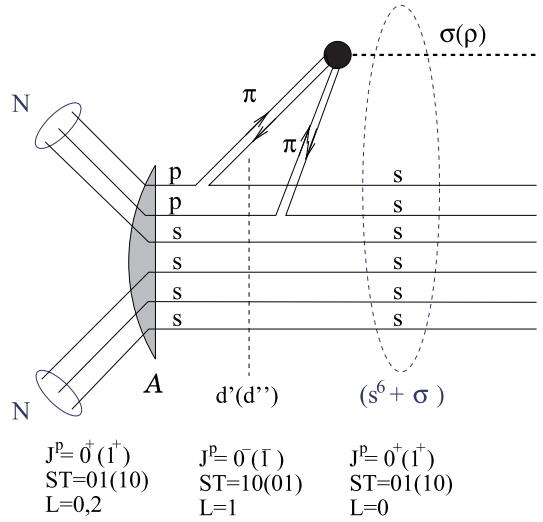

Fig. B1. The transition from the NN to the dressed bag channel via two sequential pion emissions from two p-shell quarks.

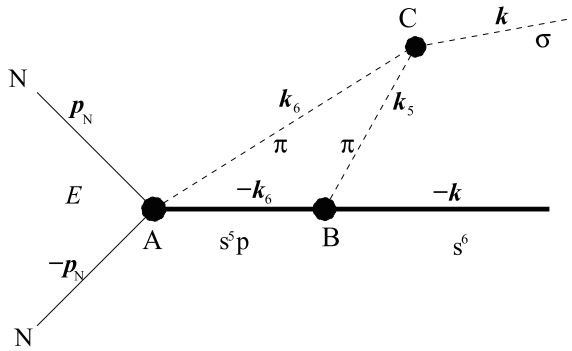

Fig. B2. Triangle diagram corresponding to the σ-meson formation from two pions in the transition of two p-shell quarks to the s orbit (k_5 and k_6 are the momenta of the 5-th and 6-th quarks in the diagram of Fig. B1).

in a simplified form as a triangular diagram that does not explicitly contain the quark lines (see Fig. B2).

As can be seen from these diagrams, to calculate the respective amplitude, it is necessary to determine three vertices (A, B and C) and carry out the integration over the momenta $\boldsymbol{k}_5$ and $\boldsymbol{k}_6$ of the intermediate pions emitted by the 5-th and 6-th quarks. The initial six-quark NN state is written in a form of the RGM ansatz (8) and decomposed into the basis of the TISM $6q$ configurations with two quanta of excitation (see Appendix A for detail). This decomposition includes configurations s^4p^2, s^52s, and s^5d .

At the vertex A, a transition occurs from these initial configurations to an intermediate state s^5p with the emission of a pion by one of the p-shell quarks: $s^4p^2(s^52s \text{ or } s^5d) \to s^5p+\pi$. At the vertex B, the p-shell

1) These are the quantum numbers of the so-called d' dibaryon [38]

quark of the s^5p configuration passes into the s-state with the emission of a second pion: $s^5p \to s^6 + \pi$. The pion creation amplitudes in these vertices were calculated within the framework of the well-known quark-pair-creation model [97–99] with using the TISM matrix elements for the $6q$ transitions.

The $\pi + \pi \to \sigma$ transition amplitude (the vertex C in Fig. B2) is to be proportional to the overlap of the two-pion and the σ-meson wavefunctions [100]:

$$\langle \pi(\boldsymbol{k})\pi(\boldsymbol{k}')|H_{\pi\pi\sigma}|\sigma\rangle = f_{\pi\pi\sigma}F_{\pi\pi\sigma}(\varkappa^2),$$
$$F(\varkappa^2) = \exp\left(-\frac{1}{2}\varkappa^2 b_\sigma^2\right), \tag{B2}$$

where $\varkappa = \frac{1}{2}(\boldsymbol{k} - \boldsymbol{k}')$ and b_σ is a characteristic scale of the σ meson in the $\pi\pi$ channel.

In the calculations, the shell-model quark representations for the pion and the σ meson were used [73]:

$$|\pi^\lambda\rangle = |s\bar{s}[2]_X LST = 001\, T_z = \lambda\, J^P = 0^-\rangle,$$
$$|\sigma\rangle = |s^2\bar{s}^2[4]_X, LST = 000, J^P = 0^+\rangle, \tag{B3}$$

with the Gaussian wavefunctions, e.g., $\Psi_\pi(\rho_\pi) \sim \exp(-\rho_\pi^2/4b_\pi^2)$, $\rho_\pi(ij) = \boldsymbol{r}_i - \boldsymbol{r}_j$, where b_π is the "quark radius" of the pion (≈ 0.5 $b \approx 0.3$ fm).

When calculating the triangle diagram, three possible temporal orderings of the vertices were taken into account: ABC, ACB, CBA . As a result of integration over the inner pion momentum, the explicit expressions for the vertex functions $B^J_{L_\sigma LS}(k,E)$ were obtained [8, 9]:

$$B^J_{L_\sigma LS}(k,E) = g^J_{L_\sigma LS} D^J_{L_\sigma LS}(k,E). \tag{B4}$$

Here the factor $g^J_{L_\sigma LS}$ can be considered as an effective coupling constant with the value $g^J_{0LS} = \frac{f^2_{\pi qq}}{m^2_\pi}\frac{g_{\sigma\pi\pi}}{m_q^2 b^3} C^J_{LS}$ defined in [9] at $L_\sigma = 0$. The standard coupling constants were used for the πqq and $\sigma\pi\pi$ vertices: $f_{\pi qq} = 3/5 f_{\pi NN}$ and $g_{\sigma\pi\pi} \approx 2$–$4$ GeV$/c$, while the parameters C^J_{LS} were calculated by the f.p.c. technique. The vertex functions $D^J_{0LS}(k,E)$ are rather cumbersome expressions that include the integration over the inner momenta of the diagram in Fig. B2. We do not present these vertex functions here, since the definition of the effective potential $w(E)$ for the external channel includes only their convolutions with the meson propagator, which determine the energy-dependent coupling constants $\lambda^J_{LL'}(E)$ (42). To approximately reproduce the energy dependence of the constants $\lambda^J_{LL'}(E)$ derived from the microscopic calculation, the Pade approximant [1, 1] was used in Refs. [8, 9] and in subsequent applications of the dibaryon model.

References

[1] S. Aoki and T. Doi, Front. Phys. **8**, 307 (2020)
[2] F. Fernandez, P.G. Ortega, and D.R. Entem, Front. Phys. **7**, 233 (2020)
[3] V.I. Kukulin, Phys. Atom. Nucl. **74**, 1567 (2011)
[4] H. Clement, Prog. Part. Nucl. Phys. **93**, 195 (2017)
[5] H. Clement and T. Skorodko, Chin. Phys. C **45**(2), 022001 (2021).
[6] A. Gal, Acta Phys. Polon. B **47**, 471 (2016)
[7] V.I. Kukulin, in: *Proceedings of XXXIII Winter School PIYaF,* Gatchina, 1999, p. 207
[8] V.I. Kukulin, I.T. Obukhovsky, V.N. Pomerantsev *et al.*, J. Phys. G **27**, 1851 (2001)
[9] V.I. Kukulin, I.T. Obukhovsky, V.N. Pomerantsev *et al.*, Int. J. Mod. Phys. E **11**, 1 (2002)
[10] M.I. Krivoruchenko and A. Faessler, Rom. J. Phys. **57**, 296 (2012)
[11] V.I. Kukulin and M.N. Platonova, Phys. At. Nucl. **76**, 1465 (2013)
[12] V.I. Kukulin *et al.*, Ann. Phys. (NY) **325**, 173 (2010)
[13] V.I. Kukulin, V.N. Pomerantsev, O.A. Rubtsova *et al.*, Phys. At. Nucl. **82**, 934 (2019)
[14] V.I. Kukulin *et al.*, Phys. Lett. B **801**, 135146 (2020)
[15] V.I. Kukulin *et al.*, Eur. Phys. J. A **56**, 229 (2020)
[16] O.A. Rubtsova, V.I. Kukulin, and M.N. Platonova, Phys. Rev. D **102**, 114040 (2020)
[17] F.J. Dyson and N.-H. Xuong, Phys. Rev. Lett. **13**, 815 (1964); Erratum *ibid.* **14**, 339 (1965)
[18] M.G. Meshcheriakov, B.S. Neganov, Dokl. Akad. Nauk SSSR **100**, 677 (1955)
[19] B.S. Neganov, L.B. Parfenov, Soviet Phys. JETP **7**, 528 (1958)
[20] N. Hoshizaki, Prog. Theor. Phys. **60**, 1796 (1978)
[21] N. Hoshizaki, Prog. Theor. Phys. **61**, 129 (1979)
[22] N. Hoshizaki, Prog. Theor. Phys. **89**, 251 (1993)
[23] N. Hoshizaki, Prog. Theor. Phys. **89**, 569 (1993)
[24] R. Bhandari, R.A. Arndt, L.D. Roper *et al.*, Phys. Rev. Lett. **46**, 1111 (1981)
[25] C.-H. Oh, R.A. Arndt, I.I. Strakovsky *et al.*, Phys. Rev. C **56**, 635 (1997)
[26] A.V. Kravtsov, M.G. Ryskin, and I.I. Strakovsky, J. Phys. G **9**, L187 (1983)
[27] I.I. Strakovsky, A.V. Kravtsov, and M.G. Ryskin, Sov. J. Nucl. Phys. **40**, 273 (1984)
[28] A. Gal and H. Garcilazo, Nucl. Phys. A **928**, 73 (2014)
[29] A. Gal and H. Garcilazo, Phys. Rev. Lett. **111**, 172301 (2013)
[30] T. Kamae *et al.*, Phys. Rev. Lett. **38**, 468 (1977)
[31] T. Kamae and T. Fujita, Phys. Rev. Lett. **38**, 471 (1977)
[32] M. Bashkanov *et al.* (CELSIUS/WASA Collaboration), Phys. Rev. Lett. **102**, 052301 (2009)
[33] P. Adlarson *et al.* (WASA-at-COSY Collaboration), Phys. Rev. Lett. **106**, 242302 (2011)
[34] P. Adlarson et al. (WASA-at-COSY Collaboration), Phys. Lett. B **721**, 229 (2013)
[35] P. Adlarson *et al.* (WASA-at-COSY Collaboration and SAID Data Analysis Center), Phys. Rev. Lett. **112**, 202301

(2014)
[36] P. Adlarson *et al.* (WASA-at-COSY Collaboration and SAID Data Analysis Center), Phys. Rev. C **90**, 035204 (2014)
[37] P. Adlarson *et al.* (WASA-at-COSY Collaboration and SAID Data Analysis Center), Phys. Rev. C **102**, 015204 (2020)
[38] M. Bashkanov *et al.* (A2 Collaboration), Phys. Rev. Lett. **124**, 132001 (2020)
[39] M. Bashkanov *et al.*, Phys. Lett. B **789**, 7 (2019) and references therein
[40] M. Bashkanov, S.J. Brodsky, and H. Clement, Phys. Lett. B **727**, 438 (2013)
[41] F. Huang, Z.Y. Zhang, P.N. Shen *et al.*, Chin. Phys. C **39**, 071001 (2015)
[42] F. Huang, P.N. Shen, Y.B. Dong *et al.*, Sci. China Phys. Mech. Astron. **59**, 622002 (2016)
[43] J.A. Niskanen, Phys. Rev. C **95**, 054002 (2017)
[44] P. Adlarson *et al.* (WASA-at-COSY Collaboration), Phys. Rev. Lett. **121**, 052001 (2018)
[45] P. Adlarson *et al.* (WASA-at-COSY Collaboration), Phys. Rev. C **99**, 025201 (2019)
[46] P. Adlarson *et al.* (WASA-at-COSY Collaboration), Phys. Lett. B **762**, 455 (2016)
[47] I.P. Auer *et al.*, Phys. Lett. B **67**, 113 (1977)
[48] I.P. Auer *et al.*, Phys. Lett. B **70**, 475 (1977)
[49] K. Hidaka *et al.*, Phys. Lett. B **70**, 479 (1977)
[50] I.P. Auer *et al.*, Phys. Rev. Lett. **41**, 354 (1978)
[51] I.P. Auer *et al.*, Phys. Rev. Lett. **41**, 1436 (1978)
[52] I.P. Auer *et al.*, Phys. Rev. Lett. **48**, 1150 (1982)
[53] M.H. MacGregor, Phys. Rev. D **20**, 1616 (1979)
[54] P.J. Mulders, A.T.M. Aerts, and J.J. De Swart, Phys. Rev. D **21**, 2653 (1980)
[55] L.A. Kondratyuk, B.V. Martemyanov, and M.G. Shchepkin, Sov. J. Nucl. Phys. **45**, 776 (1987)
[56] W. Brodowski *et al.*, Z. Phys. A **355**, 5 (1996)
[57] W. Brodowski *et al.*, Phys. Lett. B **550**, 147 (2002)
[58] R.L. Workman, W.J. Briscoe, and I.I. Strakovsky, Phys. Rev. C **94**, 065203 (2016); all SAID PWA solutions can be accessed via the website: http://gwdac.phys.gwu.edu
[59] V. Komarov *et al.*, Phys. Rev. C **93**, 065206 (2016)
[60] M.N. Platonova and V.I. Kukulin, Nucl. Phys. A, **946**, 117 (2016)
[61] M.N. Platonova and V.I. Kukulin, Phys. Rev. D, **94**, 054039 (2016)
[62] I.I. Strakovsky, Fiz. Elem. Chast. Atom. Yadra, **22**, 615 (1991)
[63] I.I. Strakovsky, AIP Conf. Proc. **221**, 218 (1991)
[64] J.A. Niskanen, Phys. Rev. C **102**, 024002 (2020)
[65] H. Clement and T. Skorodko, arXiv: 2010.09217[nucl-ex]
[66] H. Clement, priv. comm.
[67] T. Ishikawa *et al.*, Phys. Lett. B **789**, 413 (2019)
[68] Y. Toyama *et al.* (NKS2 Collaboration), Few-Body Syst. **63**, 15 (2022)
[69] T. Ishikawa *et al.*, Phys. Rev. C **104**, L052201 (2021)
[70] D. Tsirkov *et al.*, EPJ Web Conf. **199**, 02016 (2019)
[71] D. Alde *et al.* (GAMS Collaboration), Phys. Lett. B **397**, 350 (1997)
[72] M.N. Platonova and V.I. Kukuin, Phys. Rev. C **87**, 025202 (2013)
[73] M.N. Platonova and V.I. Kukulin, Phys. Rev. D **103**, 114025 (2021)
[74] E. Eichten, S. Godfrey, H. Mahlke, and J.L. Rosner, Rev. Mod. Phys. **80**, 1161 (2008)
[75] A.M. Kusainov, V.G. Neudatchin, and I.T. Obukhovsky, Phys. Rev. C **44**, 2343 (1991)
[76] I.T. Obukhovsky and A.M. Kusainov, Phys. Lett. B **238**, 142 (1990)
[77] P.A. Zyla *et al.* (Particle Data Group), Prog. Theor. Exp. Phys. **2020**, 083C01 (2020)
[78] L.Ya. Glozman, Phys. Lett. B **475**, 329 (2000)
[79] L.Ya. Glozman and A.V. Nefediev, Phys. Rev. D **76**, 096004 (2007)
[80] M.K. Volkov, A.E. Radzhabov, and N.L. Russakovich, Phys. At. Nucl. **66**, 997 (2003)
[81] M.K. Volkov *et al.*, Phys. Lett. **B424**, 235 (1998)
[82] S. Saito, Prog. Theor. Phys. **41**, 705 (1969)
[83] I.T. Obukhovsky, Prog. Part. Nucl. Phys. **36**, 359 (1996)
[84] M. Harvey, Nucl. Phys. A **352**, 301 (1981)
[85] M. Harvey, Nucl. Phys. A **352**, 326 (1981)
[86] I.T. Obukhovsky, V.G. Neudatchin, Yu.F. Smirnov *et al.*, Phys. Lett. B **88**, 231 (1979)
[87] A. De Rujula, H. Georgi, and S.L. Glashow, Phys. Rev. D **12**, 147 (1975)
[88] V.G. Neudatchin, I.T. Obukhovsky, V.I. Kukulin *et al.*, Phys. Rev. C **11**, 128 (1975)
[89] V.G. Neudatchin, Yu.F. Smirnov, and R. Tamagaki, Prog. Theor. Phys. **58**, 1072 (1977)
[90] V.M. Krasnopolsky, V.I. Kukulin, V.N. Pomerantsev *et al.*, Phys. Lett. B **165**, 7 (1985)
[91] V.I. Kukulin, V.N. Pomerantsev, M. Kaskulov *et al.*, J. Phys. G **30**, 287 (2004)
[92] V.I. Kukulin, V.N. Pomerantsev, and A. Faessler, J. Phys. G **30**, 309 (2004)
[93] V.N. Pomerantsev, V.I. Kukulin, V.T. Voronchev *et al.*, Phys. Atom. Nucl. **68**, 1453 (2005)
[94] M. Kakenov, V.I. Kukulin, V.N. Pomerantsev *et al.*, Eur. Phys. J. A **56**, 266 (2020)
[95] I.T. Obukhovsky, A. Faessler, D.K. Fedorov *et al.*, Phys. Rev. D **84**, 014004 (2011)
[96] I.T. Obukhovsky, A. Faessler, D.K. Fedorov *et al.*, Phys. Rev. D **100**, 014032 (2019)
[97] A. Le Yaouanc, L. Oliver, O. Péne *et al.*, *Hadron Transitions in the Quark Model* (Gordon and Beach Science Publishers, NY), 1988
[98] F. Cano, F. González, S. Noguera *et al.*, Nucl. Phys. A **603**, 257 (1996)
[99] J. Carbonell, B. Deplanques, V.A. Karmanov *et al.*, Phys. Rep. **300**, 215 (1998)
[100] T. Gutsche, R.D. Viollier, and A. Faessler, Phys. Lett. B **331**, 8 (1994)